Mathematical Institute

Peter Julius Waldert, BSc BSc

Wolfson College

General Kernel Spectral Methods for Equilibrium Measures

MASTER'S THESIS

a thesis submitted for the degree of

Master of Science (MSc)

in

Mathematical Modelling and Scientific Computing (MMSC)

submitted to the

University of Oxford

Academic Supervisors

Dr. Timon Gutleb[a]

Prof. José A. Carrillo de la Plata MA, FEurASc, FSIAM, MAE, FIMA[a]

[a]Mathematical Institute, University of Oxford

Oxford, August 2023

Abstract

This MMSC thesis with a catchy abstract will explore general kernel spectral methods for finding equilibrium measures where initial progress was made in Gutleb, José A. Carrillo and S. Olver 2022b and Gutleb, José A. Carrillo and S. Olver 2022a.

To be done / included.

Statement of Originality: The extension of the attractive-repulsive kernel spectral method into a general kernel spectral method along with an implementation of it is original. All code contributions, starting from the particle simulation software to the implementation of the spectral methods, are entirely original.

Keywords: Pairwise Interaction Potentials, Many-Body Systems, Particle Simulations, Swarming Behaviours, Equilibrium Measures, Spectral Methods, Orthogonal Polynomials, Numerical Analysis

Languages: C++, Julia, Python

Acknowledgements

Contents

Chapter 1

Introduction

This chapter will give a brief overview of the setting of the problem considered in this dissertation, motivate a few biological and physical examples, and set up some notational conventions.

1.1 Problem Setting

The present thesis is concerned with many-body systems, treating particles in an abstract sense as they could take the form of physical atoms, birds in a flock or fish in a school. Other examples include ant colonies and swarms of insects such as locusts. A swarm of animals, a set of coordinated entities, brings many advantages for its members. For example, they share water resistance or it is easier to find a mate within the swarm than otherwise. They also often mimic larger animals to fend off predators and swarming behaviour ("swarm intelligence") plays an important role in this process. There are some disadvantages as well, like the accelerated spread of diseases or when resources are scarce, some swarm species even begin cannibalistic behaviour (D'Orsogna 2017).

From a more physical perspective, pair potentials $K : \mathbb{R}^+ \mapsto \mathbb{R}$ provide a simple and computationally efficient way to approximate the interaction between two particles based solely on their distance (cf. Figure 1.1a as a simple illustration). Pairwise potentials can be used to approximate a wide range of interactions, including interatomic potentials in physics and computational chemistry. Common examples of pair potentials include the Lennard-Jones potential and the Morse potential, which are widely used in molecular dynamics simulations to study the behaviour of atoms and

molecules, as well as the Coulomb potential used to describe the interaction between two charges in electrodynamics.
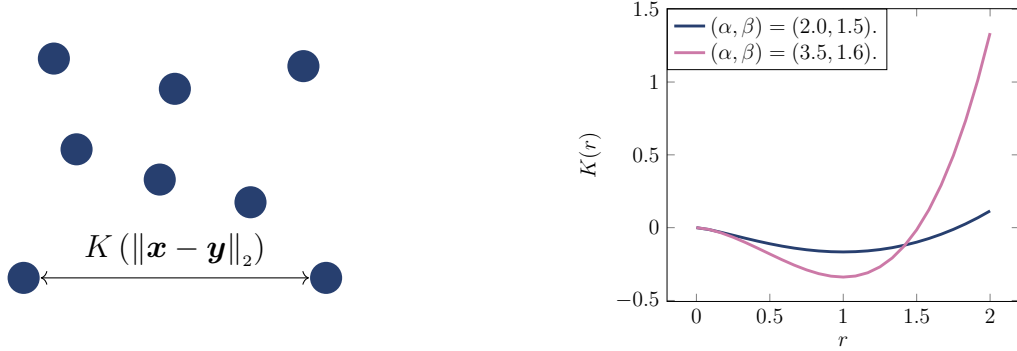
(a) $N = 8$ particles interacting with one another through the potential $K(r)$.

(b) Plot of attractive-repulsive potential functions $K_{\alpha,\beta}(r) = \frac{r^\alpha}{\alpha} - \frac{r^\beta}{\beta}$ for different α, β.

From here on, we will refer to said swarm entities, be it fish, birds or atoms, as *particles*.

Fractional differential operators act non-locally, contrary to a regular derivative which tells us very local behaviour of a function at one point. Changes far away from that point do not affect a regular derivative, while they certainly do affect a fractional derivative such as the fractional Laplacian. In the context of Partial Differential Equation (PDE)s where equations are often set in terms of time, it is often said that fractional derivatives have "memory".

1.2   Notational Conventions

Let $\mathbb{N}$ denote the natural numbers (positive integers) without 0 and let $\mathbb{N}_0 := \mathbb{N} \cup \{0\}$. In the following, we will use **bold** notation for vectors, matrices will generally be denoted by a capital letter and scalars by a lowercase letter. We will frequently make use of the (Euclidean) 2-norm of a vector, as denoted by $\|\cdot\|_2$. So for a d-dimensional vector $\boldsymbol{x} \in \mathbb{R}^d$ with entries $x_1, ..., x_d \in \mathbb{R}$ we have $\|\boldsymbol{x}\|_2 := \sqrt{\sum_{k=1}^d x_k^2}$. Also note that for readability, we will use the notation $\boldsymbol{x}^2 := \boldsymbol{x}^T \boldsymbol{x} = \|\boldsymbol{x}\|_2^2 \in \mathbb{R}^+$. Let $\boldsymbol{e}_1 := (1, 0, ..., 0)^T$ denote the unit vector in the direction of the first dimension. Let δ_{ij} denote the Kronecker delta with $\delta_{ij} = 1$ when $i = j$ and 0 otherwise.

One should also clarify the nature of a few of the integrals appearing in this thesis which are often performed over the closed unit ball $B_1(\boldsymbol{x}) := \{\boldsymbol{y} \in \mathbb{R}^d \mid \|\boldsymbol{x} - \boldsymbol{y}\|_2 \leq 1\}$ centered at the origin $\boldsymbol{x} = \boldsymbol{0}$. These volume integrals (often ended by $\mathrm{d}^d y$ or $\mathrm{d}V$) over

the d-dimensional unit ball shall be written as

$$\int_{B_1(\mathbf{0})} \mathrm{d}\boldsymbol{y}\,,$$

where $\boldsymbol{y} \in \mathbb{R}^d$ is the integration variable. Note that some definitions of $B_1(\boldsymbol{x})$ are open sets, leaving out the shell $\{\boldsymbol{y} \in \mathbb{R}^d \mid \|\boldsymbol{x} - \boldsymbol{y}\|_2 = 1\}$. The choice of definition does not matter for our purposes as the shell, a hyperplane of Lebesgue measure 0, does not contribute to the integral.

All numerical plots and figures in this thesis were generated using the Makie visualisation tool (Danisch and Krumbiegel 2021), an open-source package available for the Julia computing language (Bezanson et al. 2017).

Chapter 2

Particle Interaction Theory

As mentioned in the introduction.

2.1   A Many-Body System

is a set of particles with position and velocity interacting with one another. Each particle individually is subject to inertia and its kinetic energy ("second moment" [1]) is given by

$$E_{\text{kin},i} = \frac{\hat{\boldsymbol{p}}_i^2}{2m} = \frac{(m\hat{\boldsymbol{v}}_i)^2}{2m} = \frac{1}{2}m \left\| \hat{\boldsymbol{v}}_i \right\|_2^2 .$$

The second important ingredient is an interaction potential motivating pairwise forces $\boldsymbol{F_{ij}} \in \mathbb{R}^d$ between particles

$$\boldsymbol{F}_{ij} = -\nabla U_{ij} = - \left(\partial x_1, ..., \partial x_d \right)^T U_{ij} .$$

The total potential of a system of $N_p \geq 2$ particles $U \in \mathbb{R}$ can be calculated by summing up the pair potentials $U_{ij} \in \mathbb{R}$ between all pairs of particles

$$U = \sum_{i=1}^{N_p} \sum_{j=1,j\neq i}^{N_p} U_{ij} = \sum_{i=1}^{N_p} \sum_{j=1,j\neq i}^{N_p} K \left(\left\| \hat{\boldsymbol{x}}_i - \hat{\boldsymbol{x}}_j \right\|_2 \right) ,$$

where $\hat{\boldsymbol{x}}_i \in \mathbb{R}^d$ represents the d-dimensional position of particle i, respectively.

In the absence of an external potential V, the total energy is given by $E = E_{\text{kin}} + U$, so

$$E = \frac{1}{2} \sum_{i=1}^{N_p} m_i \hat{\boldsymbol{v}}_i^2 + \sum_{i=1}^{N_p} \sum_{j=1,j\neq i}^{N_p} K \left(\left\| \hat{\boldsymbol{x}}_i - \hat{\boldsymbol{x}}_j \right\|_2 \right) . \tag{2.1}$$

---

[1]In kinetic theory, the 0th moment is the mass m_i of a particle, the first moment is the momentum $\hat{\boldsymbol{p}}_i$ and the second moment is its kinetic energy $E_{kin,i}$.

Each particle $i = 1, ..., N_p$ at position $\hat{\boldsymbol{x}}_i \in \mathbb{R}^d$ and time $t \in \mathbb{R}^+$ then follows

$$\frac{\mathrm{d}^2\hat{\boldsymbol{x}}_i}{\mathrm{d}t^2} = f\left(\left\|\frac{\mathrm{d}\hat{\boldsymbol{x}}_i}{\mathrm{d}t}\right\|_2\right)\frac{\mathrm{d}\hat{\boldsymbol{x}}_i}{\mathrm{d}t} - \frac{1}{N}\sum_{j=1,i\neq j}^{N}\nabla K\left(\|\hat{\boldsymbol{x}}_i - \hat{\boldsymbol{x}}_j\|_2\right), \tag{2.2}$$

for reference see, for example, (Gutleb, José A. Carrillo and S. Olver 2022b; Gutleb, José A. Carrillo and S. Olver 2022a). For now, we only consider the case without an external potential $V(\hat{\boldsymbol{x}})$.

2.2   Continuous Limit

The evolution equation, in the continuous limit as $N_p \to \infty$, becomes

$$\frac{\partial\hat{\rho}}{\partial t} = \nabla \cdot (\hat{\rho}\nabla K * \hat{\rho}). \tag{2.3}$$

where $\hat{\rho} : \mathbb{R} \mapsto \mathbb{R}$ is the particle density function.

Proof. **To be done / included.**

$\square$

The solution $\hat{\rho}$ we are looking for within the scope of this dissertation is the *equilibrium measure* (cf. Definition 2.1) minimising the total potential U.

Definition 2.1: Equilibrium Measure

For a given pairwise interaction potential $K : \mathbb{R} \mapsto \mathbb{R}$, the equilibrium measure $\hat{\rho} : D \mapsto \mathbb{R}$ with $D \subseteq \mathbb{R}^d$ is a measure chosen such that

$$U_K[\hat{\rho}] := \frac{1}{2}\iint K\left(\|\hat{\boldsymbol{x}} - \hat{\boldsymbol{y}}\|_2\right)\,\mathrm{d}\hat{\rho}(\hat{\boldsymbol{x}})\,\mathrm{d}\hat{\rho}(\hat{\boldsymbol{y}}),$$

is minimised, where $\mathrm{d}\hat{\rho} = \hat{\rho}(\hat{\boldsymbol{x}})\mathrm{d}\hat{\boldsymbol{x}}$.

Also consider the total mass of the equilibrium distribution, given by

$$M[\hat{\rho}] := \int \mathrm{d}\hat{\rho} = \int_{\mathrm{supp}(\hat{\rho})}\hat{\rho}(\hat{\boldsymbol{x}})\,\mathrm{d}\hat{\boldsymbol{x}}, \tag{2.4}$$

which, without loss of generality, we can choose as $M = 1$ to make $\hat{\rho}(\hat{\boldsymbol{x}})$ a *probability distribution*. Also note that, as the integrand of the above integrals, we sometimes refer to the interaction potential K as an integral kernel or simply *kernel*.

Due to the absence of an external potential, solutions usually have translational invariance, so one might as well choose them to be centered at the origin (i.e. on $D = B_R(\mathbf{0})$ instead of $B_R(\hat{\boldsymbol{x}}_{\text{centre}})$).

As throughout the rest of this document, we will restrict ourselves to radially symmetric solutions we will use $\hat{\boldsymbol{x}} := R\hat{\boldsymbol{x}} \in B_R(\mathbf{0})$ to denote position in the original d-dimensional ball domain of radius R, whereas $x \in B_1(\mathbf{0})$ denotes position in the normalised domain with radius 1. Solutions on the original domain shall be denoted by $\hat{\rho} \in \hat{\mathcal{L}}$ whereas equilibrium measures $\rho \in \mathcal{L}$ denote solutions on the normalised domain $B_1(\mathbf{0})$ with $\mathcal{L}$ and $\hat{\mathcal{L}}$ given in Definition 2.2. Therefore, $\operatorname{supp}(\hat{\rho}) = B_1(\mathbf{0})$ and $\operatorname{supp}(\rho) = B_R(\mathbf{0})$. Of course, $\hat{\rho}(\hat{\boldsymbol{x}}) = \hat{\rho}(R\boldsymbol{x}) = \rho(\boldsymbol{x})$.

> **Definition 2.2: Solution Space**
>
> On the original domain $B_R(\mathbf{0}) \subset \mathbb{R}^d$, let $\hat{\mathcal{L}} := \{\rho : B_R(\mathbf{0}) \mapsto \mathbb{R}\}$, which can be equivalently written on the normalised domain $B_1(\mathbf{0})$: $\mathcal{L} := \{\rho : B_1(\mathbf{0}) \mapsto \mathbb{R}\}$.

> **Definition 2.3: Power-Law Potential**
>
> For a given equilibrium measure $\rho \in \mathcal{L}$ and $\beta \in \mathbb{R}$, let
>
> $$U^{(\beta)}[\rho] := \iint \|\boldsymbol{x} - \boldsymbol{y}\|_2^\beta \, \mathrm{d}\rho(\boldsymbol{x})\mathrm{d}\rho(\boldsymbol{y}) \,.$$

Note that because

$$\iint \|\boldsymbol{x} - \boldsymbol{y}\|_2^\beta \, \mathrm{d}\rho(\boldsymbol{x})\mathrm{d}\rho(\boldsymbol{y}) = \iint_{\operatorname{supp}(\rho)^2} \|\boldsymbol{x} - \boldsymbol{y}\|_2^\beta \, \rho(\boldsymbol{x})\rho(\boldsymbol{y}) \, \mathrm{d}\boldsymbol{x}\mathrm{d}\boldsymbol{y} \,,$$

this definition also generalises to $\hat{\rho} \in \hat{\mathcal{L}}$ and after a change of variables from $\boldsymbol{x}$ to $\hat{\boldsymbol{x}}$ and $\boldsymbol{y}$ to $\hat{\boldsymbol{y}}$, we obtain the relationship

$$U^{(\beta)}[\hat{\rho}] = R^{2d+\beta}U^{(\beta)}[\rho] \,.$$

With these preliminaries in mind, we can now define the problem.

> **Definition 2.4: The Problem**
>
> Finding an equilibrium measure $\hat{\rho} : B_R(\mathbf{0}) \mapsto \mathbb{R}$ of mass $M = 1$ on a d-dimensional ball of radius $R \in \mathbb{R}^+$ that minimises the total potential $U_K[\hat{\rho}]$ given an interaction kernel $K : \mathbb{R}^+ \mapsto \mathbb{R}$.

The remaining chapter will briefly discuss (analytical) approaches taken in particle physics and computational biology to solve (a version of) the above problem.

2.3   Interaction Potentials

2.3.1   Attractive-Repulsive Potential

An example we will study is that of the attractive-repulsive interaction potential, where two power law potentials compete with each other. For a given $\alpha, \beta \in \mathbb{R}\backslash\{0\}$, it is given by

$$K_{\alpha,\beta}(r) = \frac{r^\alpha}{\alpha} - \frac{r^\beta}{\beta} \, . \tag{2.5}$$

One can even consider the case when either α or β is 0 in order to arrive at a log-term (José A. Carrillo and Yanghong Huang 2017), using the convention that $\frac{x^0}{0} := \log(x)^2$. If the repulsive term is stronger (so $\beta > \alpha$), there is no equilibrium distribution as particles simply continue repelling each other out to infinity. Attractive-repulsive potentials in general describe pairwise interactions with separate attractive and repulsive terms. In our case however, we will only refer to attractive-repulsive *powerlaw* potentials, specifically of the form in Equation (2.5).

The Lennard-Jones potential ($\alpha = -12, \beta = -6$), for example, is an **intermolecular** potential, so the relevant length-scale is between molecules. Therefore, the only relevant interaction is the electromagnetic force. Other forces, such as strong force which keeps protons in the nucleus together (a force much stronger than the electromagnetic one, but with much lower reach), need not be considered at this length-scale.

2.3.2   Morse Potential

Another frequently used pairwise interaction is the *Morse potential* $K_{C_a,l_a,C_r,l_r} : \mathbb{R}^+ \mapsto \mathbb{R}$ given by

$$K_{C_a,l_a,C_r,l_r}(r) := C_a \mathrm{e}^{-r/l_a} - C_r \mathrm{e}^{-r/l_r} \, , \tag{2.6}$$

with attractive parameters $C_a \in \mathbb{R}^+$ and $l_a \in \mathbb{R}^+$ (a 'natural length scale') and repulsive parameters $C_r, l_b \in \mathbb{R}^+$. Possible parameter ranges are given by $C_a l_a^{d-2} > 1, l_a < 1$ (D'Orsogna et al. 2006; Carillo, Y. Huang and Martin 2014).

---

[2]Consider the Laurent series expansion of $\frac{x^a}{a} = \frac{1}{a} + \log(x) + \frac{1}{2} a \log^2(x) + \mathcal{O}(a^2)$ in the limit as $a \to 0^+$. While this limit approaches ∞ coming from the right and $-\infty$ coming from the left due to the nature of the first term in the expansion, the only remaining term in it is $\log(x)$ which is thereby chosen as a convention.

To be done / included.

2.3.3 Mixed Potential

2.3.4 Absolute Value Potential
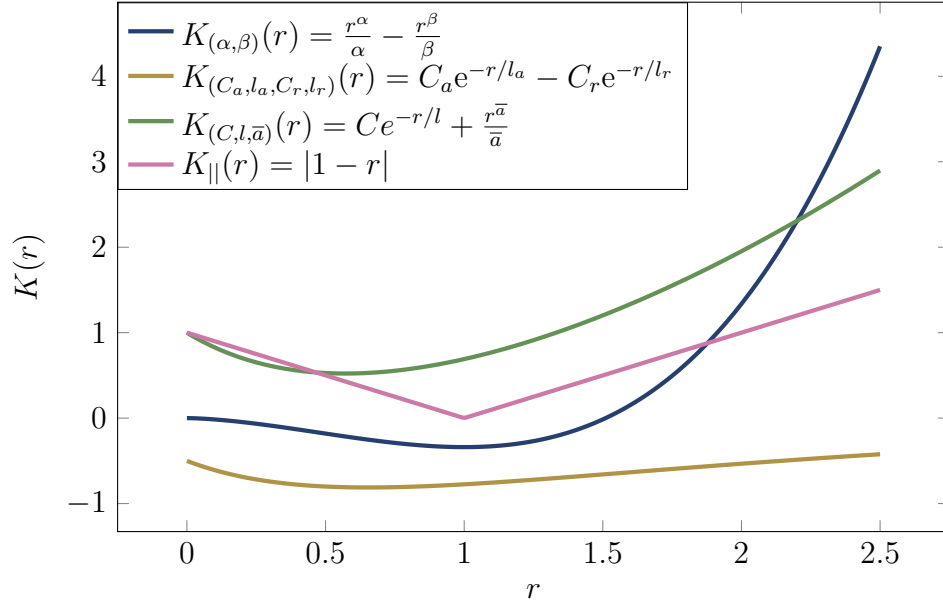
Figure 2.1: Comparing Potentials: The attractive-repulsive potential $K_{(\alpha,\beta)}(r)$ with $(\alpha,\beta) = (3.5, 1.6)$, the Morse potential $K_{(C_a,l_a,C_r,l_r)}(r)$ with $(C_a,l_a,C_r,l_r) = (1.5, 2.0, 1.0, 0.5)$, the mixed potential $K_{C,l,\overline{a}}$ with $(C,l,\overline{a}) = (1.0, 0.5, 1.8)$ and the absolute value potential $K_{||}(r)$.

2.4 Self-Propulsion and Friction

Makes it active matter. Self-propulsion and friction could be modelled as a quadratic of the form

$$f(\hat{v}_i) = 1.6 - 0.5\hat{v}_i^2 \,,$$

where $\hat{v}_i := \|\hat{\boldsymbol{v}}_i\|_2 = \left\|\frac{\mathrm{d}\hat{\boldsymbol{x}}_i}{\mathrm{d}t}\right\|_2$.

To be done / included.
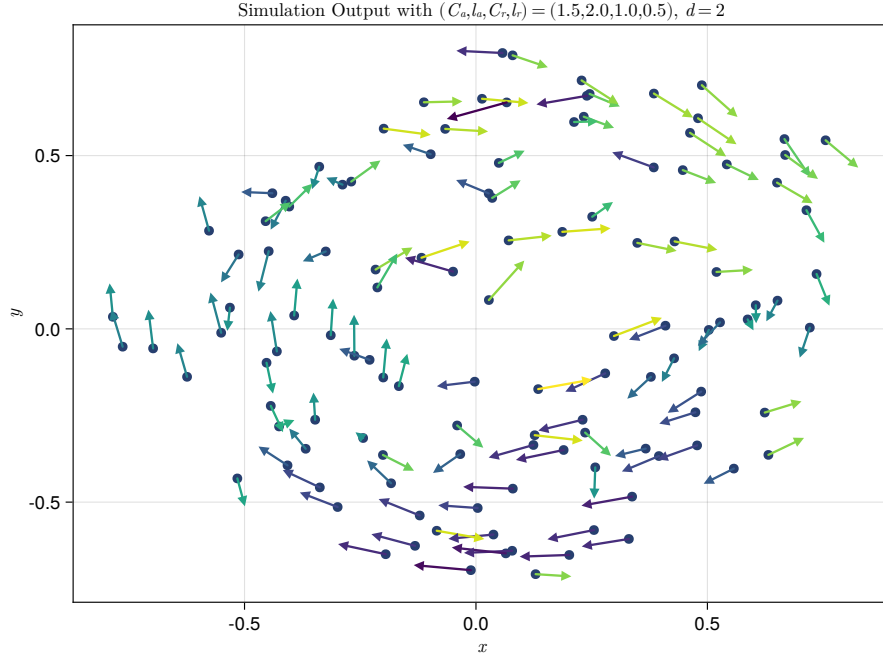
Figure 2.2: Position and velocity of $N_p = 120$ particles $d = 2$ dimensions as obtained through the molecular dynamics simulation introduced in Chapter 3. The interaction potential is a Morse potential with given parameters. Friction and self-propulsion terms are present as described in D'Orsogna et al. 2006, so using $f(v_i) = 1.6 - 0.5v_i^2$, this figure reproduces their results.

2.5   Kinetic Theory: The Vlasov Equation

A very common tool in Plasma physics.

$$\frac{\partial f}{\partial t} + \frac{\mathrm{d}\mathbf{r}}{\mathrm{d}t} \cdot \frac{\partial f}{\partial \mathbf{r}} + \frac{\mathrm{d}\mathbf{p}}{\mathrm{d}t} \cdot \frac{\partial f}{\partial \mathbf{p}} = 0,$$

This is the collisionless Boltzmann equation. Vlasov replaces the collision term with long-range interactions.

> **Theorem 2.1: Liouville's**
>
> Says that phase-space volume is conserved in situations of a pure particle-particle interaction.
> $$\frac{d\hat{\rho}}{dt} = \frac{\partial \hat{\rho}}{\partial t} + \sum_{i=1}^{n} \left(\frac{\partial \hat{\rho}}{\partial q_i} \dot{q}_i + \frac{\partial \hat{\rho}}{\partial p_i} \dot{p}_i \right) = 0 \,.$$

2.6   Vicsek Model

For the study of active matter (a number of individual agents).

<p align="center">**To be done / included.**</p>

2.7   Swarming in Biological Settings

A 2010 paper by Cavagna et al. showed the surprising result that correlation between movement of individual starlings in bird flocks over Rome is scale-free. In contrast to the assumption that birds only mirror their neighbours' behaviour and swarming behaviour emerges as a result of that, this observation suggests that bird flocks exert collective behaviour beyond local interactions.

> The change in the behavioural state of one animal affects and is affected by that of all other animals in the group, no matter how large the group is (Cavagna et al. 2010).

This work was done by individually tracking each starling in the flock and using tracking algorithms to represent their 3 dimensional positions and velocities.

2.8   Analytical Solutions

José A. Carrillo and Yanghong Huang 2017 provides some analytic solutions to the problem. For example with an attractive-repulsive potential as given in Equation (2.5), when $\alpha = 2$ and $\beta \in [-1, 2]$, the equilibrium measure is given by

$$\hat{\rho}(\hat{\boldsymbol{x}}) = C_\beta \cdot R^d \cdot \left(R^2 - \hat{\boldsymbol{x}}^2 \right)^{\frac{1-\beta}{2}} , \tag{2.7}$$

where

$$C_\beta := \frac{1}{(\beta - 1)\pi} \cos\left(\frac{(2 - \beta)\pi}{2} \right) ,$$

$$R := \left(C_\beta \cdot B\left(\frac{1}{2}, \frac{3 - \beta}{2} \right) \right)^{\frac{1}{\beta - 2}} ,$$

with $B(\cdot, \cdot)$ the beta-function (cf. Definition 4.3).

Chapter 3

Particle Simulator

The aforementioned many-body systems generally exert very complex behaviour when viewed as a whole. This behaviour can be captured in mathematical terms but also from a simulation perspective. Particle simulations have been a subject of much attention in physics and scientific computing more generally. This class of simulations, in the context of intermolecular interactions, is often referred to as molecular dynamics.
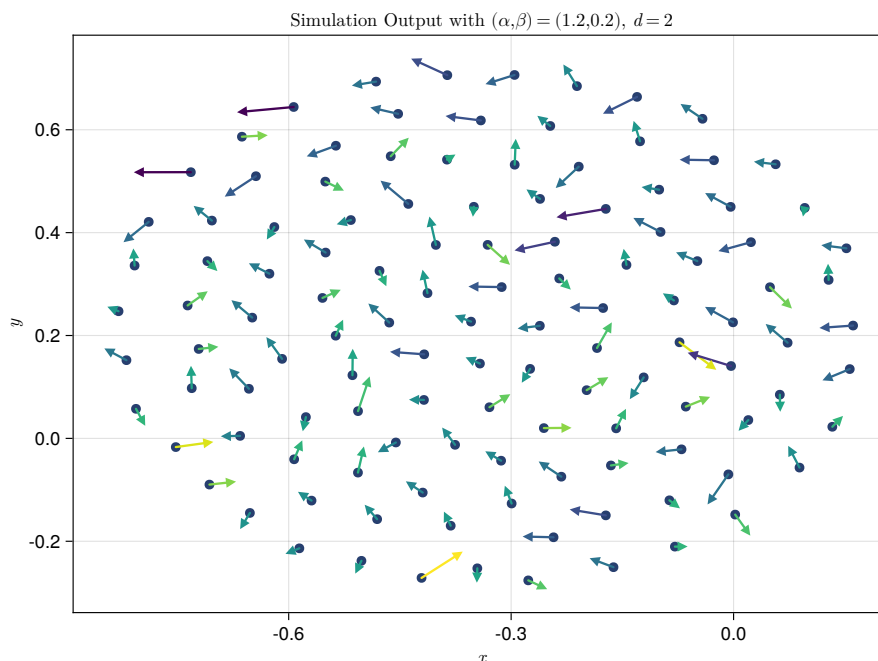
Figure 3.1: Position and velocity of particles in the simulation at a point in time. Every particle, each of equal mass m, interacts with every other particle through the interaction potential $U_{ij} = K\left(\|\boldsymbol{x_i} - \boldsymbol{x_j}\|_2\right)$ leading to $\mathcal{O}(N_p^2)$ interactions.

Because each particle interacts with every other particle, the number of interactions scales with $\mathcal{O}(N_p^2)$, which can play a prohibitive role in terms of the computation time when increasing the number of particles $N_p \gg 1$.

Within the scope of this thesis, in order to understand the elaborate behaviour of such particle systems and also to verify results from theory and the spectral method, we provide an implementation of a simulator starting from a numerical time integrator in $\mathbb{R}^d$. In addition to the *headless* simulation software, exporting state and results for treatment by the analysis component, a Graphical User Interface (GUI) is provided to enable live insight into and interaction with the model.
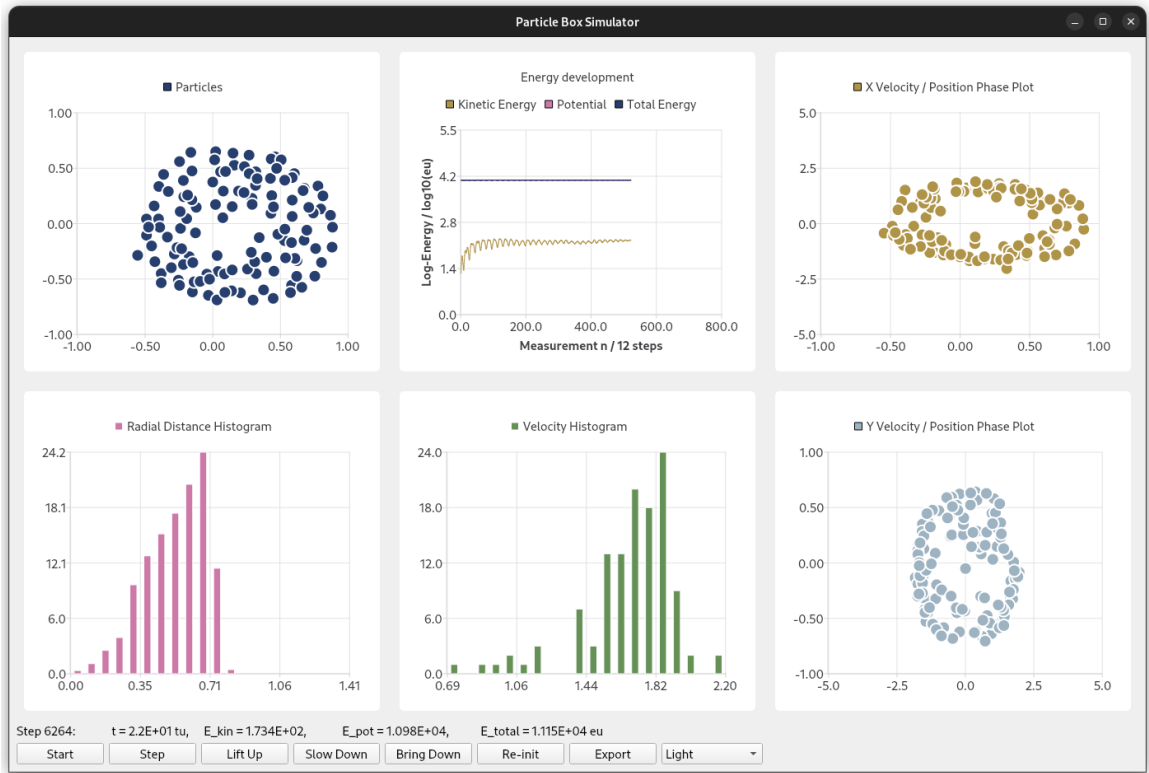
Figure 3.2: Screenshot of the GUI provided for the particle simulator. The top row shows the position of particles in their $[-1,1]^d$ ($d = 2$ in this case) domain at a point t in time, the energy development over time and the current position/velocity phase space plot. Below, there are position and velocity histogram updated live along with the simulation.
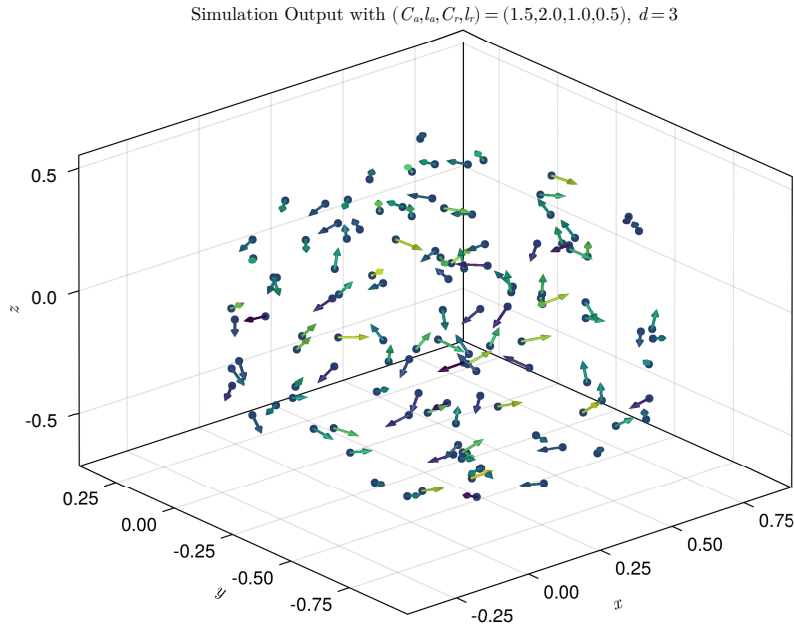
Figure 3.3: Self-propelled particles interacting via the Morse potential $K_{C_a,l_a,C_r,l_r}(r)$ in $d = 3$ dimensions.

3.1 Available Methods

As a particular important problem in the physical sciences, there is an abundant number of simulation or solution methods available for molecular dynamics problems.

Among them are simple forward integrators (e.g. $\boldsymbol{x}_i(t + \tau) \approx \boldsymbol{x}_i(t) + \tau\boldsymbol{v}_i(t)$ for $t > 0$ and timestep $\tau \in \mathbb{R}^+$), a generalisation of which are multistep methods. Both essentially originate from expanding the position and velocity as Taylor series in time. They work well in many general cases and error analysis is straightforward.

Named within the "Top 10 Algorithms of the 20th Century" (Cipra 2000), the Fast Multipole Method (FMM) due to Greengard and Rokhlin 1987 uses a multipole expansion of the system's Green's function to cluster together interactions with far-away particles for physical interaction potentials such as the Coulomb- or gravitational potentials. It does so by hierarchically clustering together particles based on position and treating interaction with far-away particles as a single interaction, therefore reducing the runtime from $\mathcal{O}(N_p^2)$ for each pair of particles down to $\mathcal{O}(N_p)$. FMM is among the few methods with rigorous results available on the error. For long-range interactions however, as they are ubiquitous within this thesis (cf. the summary in Figure 2.1), the FMM is not applicable.

Another specialised method for the integration of Newton's equations of motion is leapfrog integration, our method of choice for the C++ implementation of the N_p-body simulator.

3.1.1   Leapfrog Integration

The Leapfrog algorithm is a more effective forward integration method due to its high resistance to numerical round-off error. Except for minor changes in the way the velocity is updated, it is essentially the same as the velocity Verlet algorithm, a variant of Verlet integration with error on the order of $\mathcal{O}(\tau^4)$ with $\tau \in \mathbb{R}^+$ the timestep.

In particular, every particle i at position $\boldsymbol{x}_i \in \mathbb{R}^d$ with velocity $\boldsymbol{v}_i \in \mathbb{R}^d$ is updated using

$$
\begin{aligned}
\boldsymbol{x}_i(t + \tau) &= \boldsymbol{x}_i(t) + \tau \cdot \boldsymbol{v}_i(t + \tau/2) && t = 0, \tau, \ldots \\
\boldsymbol{v}_i(t + \tau/2) &= \boldsymbol{v}_i(t - \tau/2) + \tau \cdot \boldsymbol{f}[\boldsymbol{x}_i(t), t] && t = \tau, 2\tau, \ldots \\
\boldsymbol{v}_i(\tau/2) &= \boldsymbol{v}_i(0) + \frac{\tau}{2} \cdot \boldsymbol{f}[\boldsymbol{x}_i(0), 0] && t = 0
\end{aligned}
$$

where $\boldsymbol{f}_i[\boldsymbol{x}_i(t), t] \in \mathbb{R}^d$ denotes the acceleration (sum of contributions of all forces divided by particle mass m_i). Verlet integration methods are a very common technique in molecular dynamics for the integration of Newton's equations of motion and implemented in many solvers. Leapfrog integration can be improved to much higher accuracy using Yoshida coefficients (Akita and F. Yoshida 1973).

3.2   Phase Space

Each particle, at every point in time t, has a position and velocity value. In $d = 1$ dimension, one can visualise both of these quantities simultaneously in a phase space plot (cf. Figure 3.4). For $d > 1$ dimension, it is possible to either only visualise the first components $\{\boldsymbol{x_i}\}_1$ and $\{\boldsymbol{v_i}\}_1$ or to visualise the norm of the position (distance from the centre of mass) $r = \|\boldsymbol{x_i} - \boldsymbol{x}_{\text{centre}}\|_2$ and velocity $\|\boldsymbol{v_i}\|_2$, where

$$
\boldsymbol{x}_{\text{centre}} := \frac{1}{N_p} \sum_{i=1}^{N_p} \boldsymbol{x_i} \,.
$$
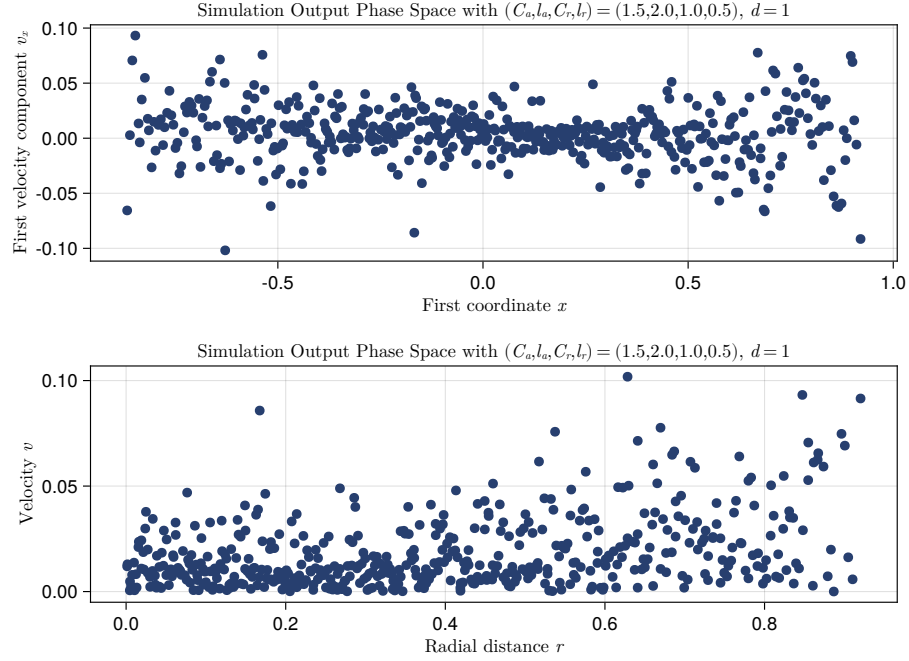
Figure 3.4: Position and velocity of $N_p = 500$ particles in a $d = 1$ simulation visualised as phase space plots using the two different visualisation mechanisms. In the top plot, one can observe natural rotation around the origin $(0, 0)$ as positive velocity corresponds to movement to the right and negative velocity to leftwards movement.

The behaviour of the phase space plot differs from potential to potential, most importantly one can observe multiple centers of rotation for the Morse potential in addition to the origin, whereas an attractive-repulsive potential builds up to an elliptical shape in the phase space plot.
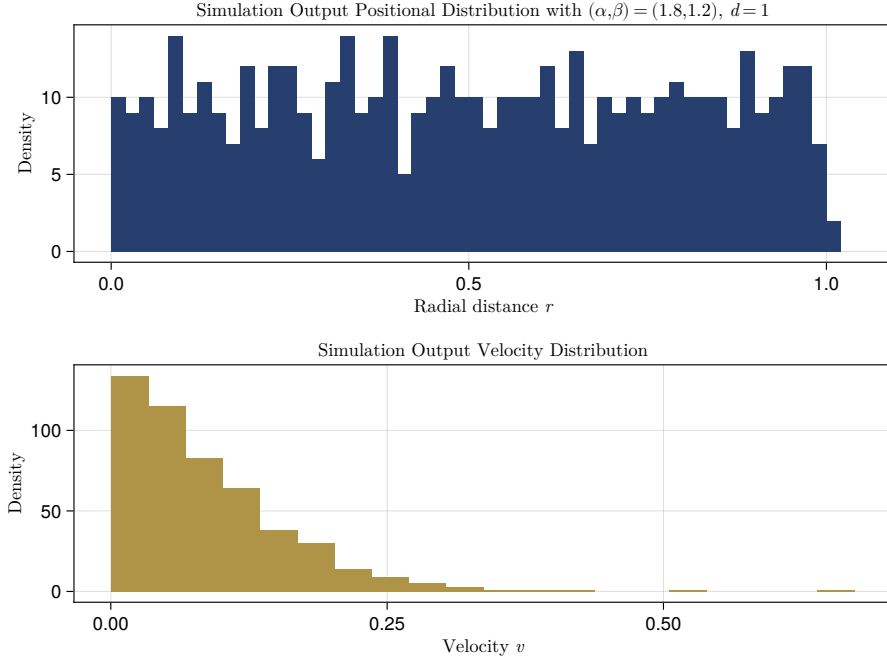
Figure 3.5: Radial Distance (r) and Velocity (v) Histograms as obtained through a long-running simulation of $N_p = 500$ particles interacting through an attractive-repulsive potential $K_{\alpha,\beta}(r)$. The spectral method introduced in Chapter 4 aims to solve for the particle density as a function of radial distance, hoping to predict the shape of the positional histogram.

In a physical setting with collision terms, the velocity distribution $f(v)$ would approach the shape of a Boltzmann distribution

$$f(v) = \left(\frac{m}{2\pi k_B T}\right)^{\frac{3}{2}} 4\pi v^2 \exp\left(-\frac{mv^2}{2k_B T}\right),$$

where k_B is the Boltzmann constant and T is temperature.

3.3   Runtime Analysis

To be done / included.

3.4   Further Experiments
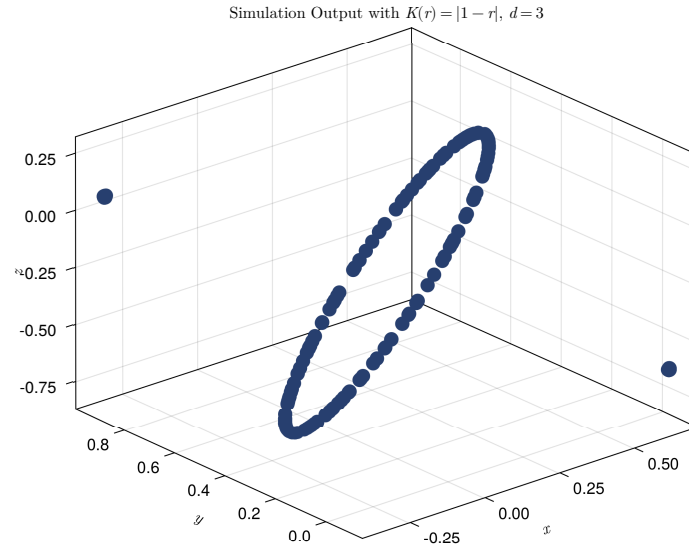
Figure 3.6: When running with $K(r) = |1 - r|$ as an interaction potential and hence, $F(r) = -\nabla K(r) = -\text{sign}(1 - r)$, in $d = 3$ dimensions a gyroscopical shape will form.
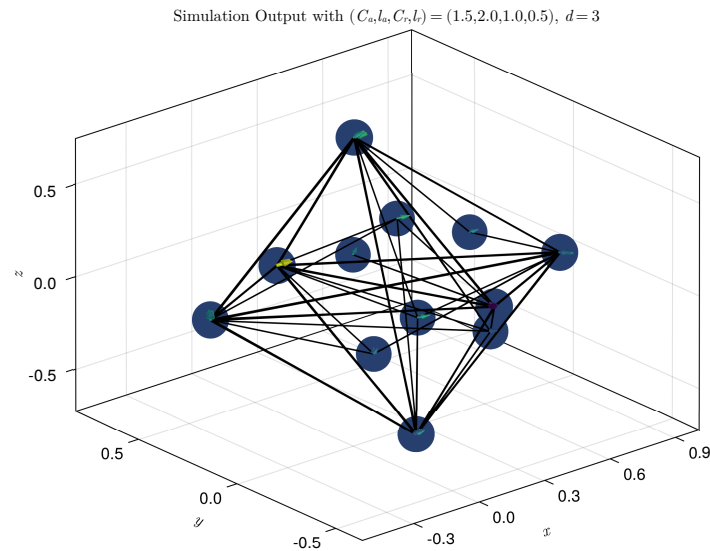
Figure 3.7: When running an $N_p = 250$ particle simulation with $K(r) = |1 - r|$ as an interaction potential in $d = 3$ dimensions the particles will align into an "optimal packing". In this case, almost equaling a face-centered cubic (fcc) array of spheres.

Chapter 4

Spectral Method

In this chapter we will construct a spectral method in the basis of Jacobi polynomials to explore the solution of equilibrium distributions $\hat{\rho}(\hat{\boldsymbol{x}})$. Starting from a many-body system and considering the continuous limit as $N_p \to \infty$, in Chapter 2 we have already established the governing equation of the particle density distribution $\hat{\rho}(\hat{\boldsymbol{x}})$ in such a system.

As mentioned in Chapter 2, the numerical approaches will be carried out on the normalised domain $B_1(\mathbf{0})$ and we will be looking for $\rho \in \mathcal{L}$, whilst in general we are interested in the $\hat{\rho} \in \hat{\mathcal{L}}$ solving our problem. Both versions are related by $\hat{\rho}(\hat{\boldsymbol{x}}) = \rho(\boldsymbol{x})$ and $\hat{\boldsymbol{x}} := R\boldsymbol{x}$.

Can we put together a numerical method to solve for the equilibrium distribution (cf. Definition 2.1)? Let us consider the problem from the bottom up and start from the solution: The basic idea behind spectral methods is to assume a solution $\rho(\boldsymbol{x})$ of the form

$$\rho(\boldsymbol{x}) = \sum_{k=0}^{N-1} \rho_k \varphi_k(\boldsymbol{x}) \,, \quad \rho_k \in \mathbb{R}, \varphi_k : \mathbb{R}^d \mapsto \mathbb{R} \,, \quad k = 0, ..., N-1 \,,$$

with N coefficients $\boldsymbol{\rho} := (\rho_0, ..., \rho_{N-1})^T$ multiplying N basis functions φ_k.

4.1   Special Functions

The following section will introduce a few necessary objects and tools to understand the basis of functions we are working with to construct the spectral method, the basis of Jacobi polynomials.

We start with the Pochhammer symbol, another name for the *rising factorial*, an unusual notation for a function but standard in the context of the special functions that will be introduced on top of it.

Definition 4.1: Rising Factorial (Pochhammer Symbol)

The nth rising factorial of $x \in \mathbb{R}$ is given by

$$(x)_n := \prod_{k=0}^{n-1} (x + k) \in \mathbb{R}.$$

For example, $(3.141)_5 = 3.141 \cdot 4.141 \cdot 5.141 \cdot 6.141 \cdot 7.141$.

Remark 4.1: When the argument is a nonpositive integer, the rising factorial $(-m)_n = -m \cdot (-m + 1) \cdot ... \cdot (-m + n - 1)$ vanishes when $n \geq m + 1$ for $n \in \mathbb{N}$ and $m \in \mathbb{N}_0$ as 0 is among the factors.

As a second prerequisite, we introduce the closely intertwined beta- and gamma-functions (Definition 4.3, Definition 4.2).

Definition 4.2: Gamma Function

Aligning with the factorial for integer arguments, $\Gamma : \mathbb{R}^+ \mapsto \mathbb{R}$ is given by

$$\Gamma(x) := \int_0^\infty t^{x-1} \mathrm{e}^{-t} \mathrm{d}t.$$

Remark 4.2: When $x \in \mathbb{R}, n \in \mathbb{N}_0$ such that $x, x + n \notin \mathbb{Z}^-$ are not negative integers, there is an important relation to the gamma function (Definition 4.2),

$$(x)_n = \frac{\Gamma(x + n)}{\Gamma(x)}.$$

Definition 4.3: Beta Function

$B : \mathbb{R}^+ \times \mathbb{R}^+ \mapsto \mathbb{R}$ is given by

$$B(x_1, x_2) := \int_0^1 t^{x_1-1}(1-t)^{x_2-1}\mathrm{d}t \,.$$

Note that following from this definition, there is a relationship with the gamma-function

$$B(x_1, x_2) = \frac{\Gamma(x_1)\Gamma(x_2)}{\Gamma(x_1 + x_2)} \,. \tag{4.1}$$

Using the Pochhammer symbol introduced in Definition 4.1, we can now define the generalised hypergeometric series $_pF_q$ (cf. Definition 4.4) and a special case of it, the Gaussian hypergeometric function (cf. Lemma 4.1).

Definition 4.4: Generalised Hypergeometric Series

The generalised hypergeometric series $_pF_q : \mathbb{R}^p \times \mathbb{R}^q \times \mathbb{C} \mapsto \mathbb{C}$ with $p, q \in \mathbb{N}$ is given by

$$_2F_1\begin{pmatrix} a_1, \ldots, a_p \\ b_1, \ldots, b_q \end{pmatrix}; z \end{pmatrix} := \sum_{k=0}^{\infty} \frac{(a_1)_k \cdots (a_p)_k}{(b_1)_k \cdots (b_q)_k} \frac{z^k}{k!} \,,$$

for $|z| < 1$ where $(\cdot)_k$ denotes the rising factorial (cf. Definition 4.1).

Note that any permutation of the first ("top") arguments $a_1, ..., a_p$ leaves the function unchanged due to commutativity of multiplication on $\mathbb{C}$. The same holds for the second ("bottom") arguments $b_1, ..., b_q$.

Lemma 4.1: Gaussian Hypergeometric Function

The $p = 2$, $q = 1$ special case of the generalised hypergeometric series, commonly referred to as the Gaussian hypergeometric function, can also be evaluated by

$$_2F_1\begin{pmatrix} a_1, -n \\ b_1 \end{pmatrix}; z \end{pmatrix} = \sum_{k=0}^{n} (-1)^k \binom{n}{k} \frac{(a_1)_k}{(b_1)_k} z^k \,,$$

when the second argument $a_2 = -n$ is a nonpositive integer, so $n \in \mathbb{N}_0$.

Proof. Starting from the definition of the generalised hypergeometric series $_pF_q$ with $p = 2$ and $q = 1$ (Definition 4.4),

$$_2F_1\begin{pmatrix} a_1, -n \\ b_1 \end{pmatrix}; z \end{pmatrix} = \sum_{k=0}^{\infty} \frac{(a_1)_k(-n)_k}{(b_1)_k} \frac{z^k}{k!} = \sum_{k=0}^{n} \frac{(a_1)_k(-n)_k}{(b_1)_k} \frac{z^k}{k!} \,,$$

which can be terminated at $k = n$ due to Remark 4.1, we can express

$$\frac{(-n)_k}{k!} = \binom{-n+k-1}{k} = (-1)^k \binom{1+n-k+k-1}{k} = (-1)^k \binom{n}{k}$$

using a well-known relation between the Pochhammer symbol and the binomial coefficient which immediately leads us to

$${}_2F_1\left(\begin{matrix} a_1, -n \\ b_1 \end{matrix}; z\right) = \sum_{k=0}^{n} \binom{n}{k} \frac{(a_1)_k}{(b_1)_k} (-z)^k \,,$$

concluding the proof. □

Note that these functions are generally tricky to evaluate efficiently, recent advancements have enabled their usage in a broader range of applications (Michel and Stoitsov 2008; Pearson, S. Olver and Porter 2017; Slevinsky 2023). Implementations are available in the HypergeometricFunctions.jl package in Julia.

More details on the Gaussian hypergeometric series, sometimes simply referred to as the hypergeometric function, its defining differential equation origin, modular interpretations and symmetries may be found in the 1997 book *Hypergeometric Functions, My Love* (M. Yoshida 1997).

4.2   Orthogonal Polynomials Forming a Basis

In order to efficiently construct a spectral method, we need an orthogonal basis.

Definition 4.5: Orthogonal Polynomials

Are univariate polynomials $p_n : \mathbb{R} \mapsto \mathbb{R}$, $p_n(x) = \sum_{k=0}^{n} c_k x^k$, $n \in \mathbb{N}_0$, forming an orthogonal basis under some inner product $\langle p_n, p_m \rangle_w$ with weight function $w(x)$, given by

$$\langle f, g \rangle_w := \int_{D_p} f(x) g(x) w(x) \, \mathrm{d}x \,,$$

the integral over some domain $D_p \subseteq \mathbb{R}$.

The domain of the integral, for all intents and purposes within this dissertation, will be the Chebyshev interval $D_p = [-1, 1]$.

Remark 4.3: The inner product satisfies $\langle x \mapsto x f(x), g \rangle_w = \langle f, x \mapsto x g(x) \rangle_w$.

Theorem 4.1: Three-Term Recurrence Relationship

All orthogonal polynomials $\{p_0, p_1, p_2, ...\}$ (cf. Definition 4.5) have (at least) a three-term recurrence relationship of the form

$$A_n p_{n+1}(x) = (B_n - x) p_n(x) + C_n p_{n-1}(x) \,.$$

Proof. Consider "$x p_n$":$= x \mapsto x p_n(x)$, a polynomial with $\deg(x p_n) \le n + 1$. By the linear independence of all orthogonal polynomials p_n with respect to the inner product $\langle \cdot, \cdot \rangle_w$, it must be possible to write

$$x p_n(x) = \sum_{k=0}^{n+1} \hat{a}_k p_k(x), \quad \text{for some } \hat{a}_k \in \mathbb{R}, k = 0, ..., n + 1 \,.$$

Now, for all $n \ge 0$ and $m \le n + 1$ we have

$$\langle x p_n, p_m \rangle_w = \sum_{k=0}^{n+1} \hat{a}_k \langle p_k, p_m \rangle_w = \sum_{k=0}^{n+1} \hat{a}_k \delta_{i,k} = \hat{a}_m \langle p_m, p_m \rangle_w \,,$$

due to the orthogonality relationship (Theorem 4.2). Therefore,

$$\hat{a}_m = \frac{\langle x p_n, p_m \rangle_w}{\langle p_m, p_m \rangle_w} \quad \text{for all } m \le n + 1 \,. \tag{4.2}$$

But when $\underline{m < n - 1}$, we have $\deg(xp_m) < n$ so $xp_m(x) = \sum_{k=0}^{n-1} \hat{b}_k p_k(x)$ for some (potentially 0) $\hat{b}_k \in \mathbb{R}$, and therefore $\langle p_n, xp_m \rangle_w = \sum_{k=0}^{n-1} \hat{b}_k \langle p_n, p_k \rangle_w = 0$, which, by the symmetry of the inner product (Remark 4.3), also implies $\langle xp_n, p_m \rangle_w = 0$ which, by Equation (4.2), allows us to conclude that the earlier coefficients $\hat{a}_m = 0$.

We recall that $xp_n(x) = \sum_{k=0}^{n+1} \hat{a}_k p_k(x)$, which in combination with our insights on the $\hat{a}_m$ above means that

$$xp_n(x) = \hat{a}_{n-1} p_{n-1}(x) + \hat{a}_n p_n(x) + \hat{a}_{n+1} p_{n+1}(x) \,,$$

concluding the proof. $\square$

For example, for the Chebyshev polynomials $T_k : [-1, 1] \mapsto \mathbb{R}$ we have

$$T_{k+1}(x) = 2xT_k(x) - T_{k-1}(x) \,.$$

Note that the converse of Theorem 4.1 is also true, a set of polynomials of increasing degree k that has a three-term recurrence relationship is a set of orthogonal polynomials (cf. Definition 4.5). While the original theorem was discovered before Favard 1935, to this day we still refer to it as *Favard's theorem.*

The Jacobi polynomials are then defined from $_2F_1$ as follows:

Definition 4.6: Jacobi Polynomials

Let $P^{(a,b)} : \mathbb{C} \mapsto \mathbb{C}$ with $a, b \in \mathbb{R}$ be given by

$$P_n^{(a,b)}(x) := \frac{(a+1)_n}{n!} \, _2F_1\left(\begin{matrix} 1+a+b+n, -n \\ a+1 \end{matrix} ; \frac{1-x}{2}\right) ,$$

using the Gaussian hypergeometric function (Lemma 4.1) and the Pochhammer symbol (Definition 4.1).

Examples: Following from this definition,

$$P_0^{(a,b)}(x) = 1$$

$$P_1^{(a,b)}(x) = (a+1) + (a+b+2)\frac{x-1}{2}$$

and so on. Also note that, as with all other orthogonal polynomials, by convention indices start at 0 and therefore $\deg\left(P_k^{(a,b)}\right) = k$.

Lemma 4.2: Jacobi Polynomial Series

Definition 4.6 of $P_n^{(a,b)}$ is equivalent to

$$P_n^{(a,b)}(x) = \frac{\Gamma(a+n+1)}{n!\,\Gamma(a+b+n+1)} \sum_{k=0}^{n} \binom{n}{k} \frac{\Gamma(a+b+n+k+1)}{\Gamma(a+k+1)} \left(\frac{x-1}{2}\right)^k,$$

where $\Gamma(x)$ is the gamma function (cf. Definition 4.2).

Proof. Inserting into Lemma 4.1, we have

$$\begin{aligned}
P_n^{(a,b)}(x) &= \frac{(a+1)_n}{n!} \sum_{k=0}^{n} (-1)^k \binom{n}{k} \frac{(1+a+b+n)_k}{(a+1)_k} \left(\frac{1-x}{2}\right)^k \\
&= \frac{\Gamma(a+1+n)}{n!\,\Gamma(a+1)} \sum_{k=0}^{n} \binom{n}{k} \frac{\Gamma(a+1)\Gamma(1+a+b+n+k)}{\Gamma(a+1+k)\Gamma(1+a+b+n)} \left(\frac{x-1}{2}\right)^k \\
&= \frac{\Gamma(a+1+n)}{n!\,\Gamma(1+a+b+n)} \sum_{k=0}^{n} \binom{n}{k} \frac{\Gamma(1+a+b+n+k)}{\Gamma(a+1+k)} \left(\frac{x-1}{2}\right)^k
\end{aligned}$$

using Remark 4.2.   □

Special Cases: The Gegenbauer (or ultraspherical) polynomials $C_n^{(\lambda)}$ are a special case of the Jacobi polynomials, namely when $a = b$, of which the Chebyshev polynomials of the first kind T_n are another special case of. Namely, when $a = b = -1/2$. The Chebyshev polynomials of the second kind U_n, once again regulated by a prefactor, are given by $a = b = +1/2$. In the special case when $a = b = 0$, the Jacobi polynomials reduce to the Legendre polynomials $P_n(x) = P_n^{(0,0)}(x)$, cf. F. Olver et al. 2018.

Dot-product notation: Note that in this manuscript we will use the dot-product notation between the vector of Jacobi polynomials and the coefficient vector,

$$f(x) = \sum_{k=0}^{N-1} f_k P_k^{(a,b)}(x) \quad \Leftrightarrow \quad f(x) = \boldsymbol{f} \cdot \boldsymbol{P}^{(a,b)}(x),$$

to express that a function f is a linear combination of basis polynomials with coefficients $\boldsymbol{f} = (f_0, ..., f_{N-1})^T \in \mathbb{R}^N$. So $\boldsymbol{P}^{(a,b)}(x) \in \mathbb{R}^N$ is the vector of Jacobi polynomials $P_0^{(a,b)}(x)$, $P_1^{(a,b)}(x)$, ..., $P_{N-1}^{(a,b)}(x)$.

Theorem 4.2: Jacobi Polynomial Orthogonality

Jacobi polynomials $P_n^{(a,b)}(x)$ are orthogonal on $D_p = [-1, 1]$ with respect to the weight function

$$w^{(a,b)}(x) = (1 - x)^a (1 + x)^b \,,$$

so they satisfy

$$\int_{-1}^{1} (1 - x)^a (1 + x)^b P_n^{(a,b)} P_m^{(a,b)} \, \mathrm{d}x = \frac{2^{a+b+1} \Gamma(a + n + 1) \Gamma(b + n + 1)}{n!(a + b + 2n + 1) \Gamma(a + b + n + 1)} \delta_{n,m} \,,$$

with $a, b > -1$, which uniquely determines $P_n^{(a,b)}(x)$.

Proof. See, for example, Arora and Bajpai 1995. $\qquad\qquad\qquad\qquad\qquad\qquad$ $\square$

As shown by, for example, "the ultraspherical method" (S. Olver and Townsend 2013), the basis of Jacobi polynomials can yield a **sparse**, and in particular, **banded** operator. This is due to the excellent property that derivatives of orthogonal polynomials and in particular, the Gegenbauer polynomials, can be expressed as tridiagonal matrices acting on coefficient space.
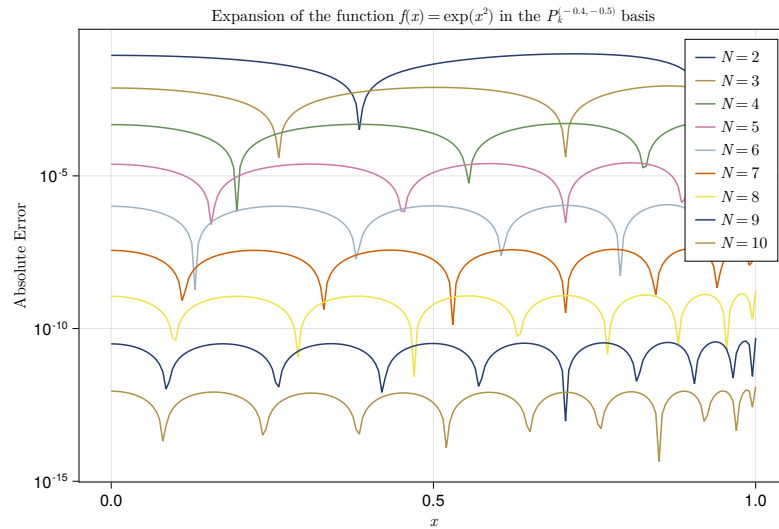
Figure 4.1: Convergence of the Jacobi polynomial expansion $f_N(x) = \sum_{k=0}^{N-1} P_k^{(a,b)}(x)$ of an example function $f(x) = \mathrm{e}^{x^2}$ with $a = -\frac{3}{4}$ and $b = -\frac{1}{2}$. Each added term improves the absolute error between the function and its expansion by a factor, so we have exponential convergence. The number of "arches" of each solution error function, occurring from the roots of $f(x) - f_N(x)$, approximately equals the order N.

An example of the approximation of a function using Jacobi polynomials is given in Figure 4.1, depicting the absolute error for expansions of growing order N.

As mentioned previously in Chapter 2, due to the absence of an external potential the solutions must be radially symmetric given that the pairwise interactions only depend on mutual distance and nothing else. So in most upcoming instances, we will work with the *radial* Jacobi polynomials, allowing us to extend the preimage of the polynomial basis from $\mathbb{R}$ to $\mathbb{R}^d$. These are simply given by $P_k^{(a,b)}\left(2\left\|\boldsymbol{x}\right\|_2^2 - 1\right)$.

> **Remark 4.4: Jacobi Matrix:** The Jacobi operator is the matrix $X \in \mathbb{R}^{N\times N}$ satisfying
> $$x \cdot \boldsymbol{P}^{(a,b)}(x) = \boldsymbol{P}^{(a,b)}(x) \cdot X^T.$$

The terms in the Jacobi operator are closely connected to the three-term recurrence relationship (cf. Theorem 4.1), even making the matrix tridiagonal.

4.3   Working Towards a Solution

Finally, now that we have established the basis functions, we can write down an ansatz $\rho : B_1(\boldsymbol{0}) \mapsto \mathbb{R}$ for the solution of the problem, of the form

$$\rho[\boldsymbol{\rho}](\boldsymbol{x}) = \rho(\boldsymbol{x}) := \left(1 - \left\|\boldsymbol{x}\right\|_2^2\right)^{m-\frac{\alpha+d}{2}} \sum_{k=0}^{N-1} \rho_k P_k^{\left(m-\frac{\alpha+d}{2}, \frac{d-2}{2}\right)}\left(2\left\|\boldsymbol{x}\right\|_2^2 - 1\right). \qquad (4.3)$$

with $P_k^{(a,b)}$ the Jacobi polynomials and $\{\rho_k\}_{k=0,\ldots,N-1}$ the coefficients.

The spectral method can then be written as a linear system of the coefficients $\boldsymbol{\rho}$ as we will see in the next section. In order to establish said linear system, we first need to introduce the *inverse fractional Laplacian*, helping us with the evaluation of the power law potential integral involving radial Jacobi polynomials given in Theorem 4.3, the most important result of this chapter.

$(-\Delta)^{-\gamma}$ denotes the inverse fractional Laplacian $\Delta := \nabla^2$ with power $\gamma \in (0,1)$. There are numerous equivalent definitions available (cf. Kwaśnicki 2017), within the context of potential theory the Riesz potential definition (Definition 4.7) is the most common.

> **Definition 4.7: Riesz Potential**
>
> For a given function $u : \mathbb{R}^d \mapsto \mathbb{R}$ and $\gamma \in \mathbb{R}$, its *Riesz potential* $I_\gamma[u]$ is given by
>
> $$I_\gamma[u](\boldsymbol{x}) := \frac{2^{-\gamma}\Gamma(\frac{d-\gamma}{2})}{\pi^{d/2}\Gamma(\gamma/2)} \int_{\mathbb{R}^d} \frac{u(\boldsymbol{z})}{\|\boldsymbol{x} - \boldsymbol{z}\|_2^{d-\gamma}} \mathrm{d}\boldsymbol{z} \,.$$

For $\gamma \in (0, d)$, the Riesz potential is equivalent to the inverse fractional Laplacian, so $(-\Delta)^{-\gamma} = I_\gamma$. So in the case of positive power law kernels, the equivalence to the inverse fractional Laplacian does not apply. Many results may still be carried over however and we move on to stating and proving Theorem 4.3.

> **Theorem 4.3: Power Law Potential of the nth Jacobi Polynomial**
>
> On the d-dimensional unit ball B_1 the power law potential, with power $\alpha \in (-d, 2 + 2m - d)$, $m \in \mathbb{N}_0$ and $\beta > -d$, of the n-th weighted radial Jacobi polynomial $(1 - \|\boldsymbol{y}\|_2^2)^{m - \frac{\alpha+d}{2}} P_n^{\left(m - \frac{\alpha+d}{2}, \frac{d-2}{2}\right)} \left(2\|\boldsymbol{y}\|_2^2 - 1\right)$ reduces to a Gaussian hypergeometric function as follows:
>
> $$I_{m,n}^{\alpha,\beta}(\boldsymbol{x}) = \int_{B_1(\boldsymbol{0})} \|\boldsymbol{x} - \boldsymbol{y}\|_2^\beta \left(1 - \|\boldsymbol{y}\|_2^2\right)^{m - \frac{\alpha+d}{2}} P_n^{\left(m - \frac{\alpha+d}{2}, \frac{d-2}{2}\right)} \left(2\|\boldsymbol{y}\|_2^2 - 1\right) \mathrm{d}\boldsymbol{y}$$
>
> $$= \frac{\pi^{d/2}\Gamma\left(1 + \frac{\beta}{2}\right)\Gamma\left(\frac{\beta+d}{2}\right)\Gamma\left(m + n - \frac{\alpha+d}{2} + 1\right)}{\Gamma\left(\frac{d}{2}\right)\Gamma(n+1)\Gamma\left(\frac{\beta}{2} - n + 1\right)\Gamma\left(\frac{\beta-\alpha}{2} + m + n + 1\right)} {}_2F_1 \left(\begin{matrix} n - \frac{\beta}{2}, -m - n + \frac{\alpha-\beta}{2} \\ \frac{d}{2} \end{matrix}; \|\boldsymbol{x}\|_2^2\right) \,.$$

Proof (adapted from Gutleb, José A. Carrillo and S. Olver 2022a). We begin by applying Lemma 4.2 to the inside of the integrand.

$$I := \int_{B_1(\boldsymbol{0})} \|\boldsymbol{x} - \boldsymbol{y}\|_2^\beta \left(1 - \|\boldsymbol{y}\|_2^2\right)^a P_n^{(a,b)} \left(2\|\boldsymbol{y}\|_2^2 - 1\right) \mathrm{d}\boldsymbol{y}$$

$$= C_{a,b,n} \sum_{k=0}^n \binom{n}{k} C_{a,b,n,k} \int_{B_1(\boldsymbol{0})} \|\boldsymbol{x} - \boldsymbol{y}\|_2^\beta \left(1 - \|\boldsymbol{y}\|_2^2\right)^a \left(\|\boldsymbol{y}\|_2^2 - 1\right)^k \mathrm{d}\boldsymbol{y}$$

$$= C_{a,b,n} \sum_{k=0}^n \binom{n}{k} C_{a,b,n,k} (-1)^k \int_{B_1(\boldsymbol{0})} \|\boldsymbol{x} - \boldsymbol{y}\|_2^\beta \left(1 - \|\boldsymbol{y}\|_2^2\right)^{a+k} \mathrm{d}\boldsymbol{y}$$

where $a := m - \frac{\alpha+d}{2}$ and $b := \frac{d-2}{2}$. Note that from the first to the second line, we used $\frac{z-1}{2} = \frac{2\|\boldsymbol{y}\|_2^2 - 1 - 1}{2} = \|\boldsymbol{y}\|_2^2 - 1$.

The constants are

$$C_{a,b,n} := \frac{\Gamma(a+1+n)}{n!\,\Gamma(1+a+b+n)}$$

$$C_{a,b,n,k} := \frac{\Gamma(1+a+b+n+k)}{\Gamma(a+1+k)}\,.$$

We identify the remaining integral as the Riesz potential $I_{\beta+d}[u](\boldsymbol{x})$, cf. Definition 4.7, of the function $u(\boldsymbol{y}) := \left(1 - \|\boldsymbol{y}\|_2^2\right)^{a+k}$, which we can evaluate using Lemma 2.4 from Biler, Imbert and Karch 2011:

$$\int_{B_1(\mathbf{0})} \|\boldsymbol{x}-\boldsymbol{y}\|_2^{\beta}\left(1-\|\boldsymbol{y}\|_2^2\right)^{a+k}\,\mathrm{d}\boldsymbol{y} = c_{\beta+d}I_{\beta+d}\left[\boldsymbol{y}\mapsto\left(1-\|\boldsymbol{y}\|_2^2\right)^{a+k}\right](\boldsymbol{x})$$

$$= c_{\beta+d}C_{a+k,\beta,d}\cdot {}_2F_1\left(\begin{matrix}\frac{d-(\beta+d)}{2},-a-k-\frac{\beta+d}{2}\\ d/2\end{matrix};\|\boldsymbol{x}\|_2^2\right)$$

$$= c_{\beta+d}C_{a+k,\beta,d}\cdot {}_2F_1\left(\begin{matrix}-\beta/2,-m-k+\frac{\alpha-\beta}{2}\\ d/2\end{matrix};\|\boldsymbol{x}\|_2^2\right),$$

as $-a-k-\frac{\beta+d}{2} = -m+\frac{\alpha+d}{2}-k-\frac{\beta+d}{2} = -m-k+\frac{\alpha-\beta}{2}$ with constants

$$c_{\beta+d} := \frac{2^{\beta+d}\pi^{d/2}\Gamma\left(\frac{\beta+d}{2}\right)}{\Gamma(-\beta/2)} \quad \text{from aforementioned definition of the Riesz potential}$$

$$C_{a+k,\beta,d} := \frac{\Gamma(a+k+1)\Gamma(-\beta/2)}{2^{\beta+d}\Gamma(d/2)\Gamma\left(a+k+\frac{\beta+d}{2}+1\right)} \quad \text{from Lemma 2.4},$$

and therefore

$$c_{\beta+d}C_{a+k,\beta,d} = \frac{2^{\beta+d}\pi^{d/2}\Gamma\left(\frac{\beta+d}{2}\right)\Gamma(a+k+1)\Gamma(-\beta/2)}{\Gamma(-\beta/2)2^{\beta+d}\Gamma(d/2)\Gamma\left(a+k+\frac{\beta+d}{2}+1\right)} = \frac{\pi^{d/2}B\left(\frac{\beta+d}{2},a+k+1\right)}{\Gamma(d/2)},$$

using Equation (4.1). So that finally,

$$\int_{B_1(\mathbf{0})}\|\boldsymbol{x}-\boldsymbol{y}\|_2^{\beta}\left(1-\|\boldsymbol{y}\|_2^2\right)^{a+k}\,\mathrm{d}\boldsymbol{y}$$

$$= \frac{\pi^{d/2}}{\Gamma(d/2)}B\left(\tfrac{\beta+d}{2},m-\tfrac{\alpha+d}{2}+k+1\right)\cdot {}_2F_1\left(\begin{matrix}-\beta/2,-m-k+\frac{\alpha-\beta}{2}\\ d/2\end{matrix};\|\boldsymbol{x}\|_2^2\right).$$

Plugging this back into the original form above, carrying along the same parameters,

$$I = C_{a,b,n}\sum_{k=0}^{n}\binom{n}{k}C_{a,b,n,k}(-1)^k\frac{\pi^{d/2}}{\Gamma(d/2)}B\left(\cdot,\cdot\right){}_2F_1\left(\ldots;\|\boldsymbol{x}\|_2^2\right)$$

we can apply Equation (2.1) in Gutleb, José A. Carrillo and S. Olver 2022a after some algebra, the special case of an identity given in Prudnikov et al. 1986 to obtain a $_3F_2$ (three terms in the numerator, two in the denominator) function

$$
I \propto {}_3F_2 \left(\begin{matrix} -\beta/2, n - \beta/2, -m - n + \frac{\alpha - \beta}{2} \\ d/2, -\beta/2 \end{matrix} ; \|\boldsymbol{x}\|_2^2 \right) ,
$$

which we expand into its Definition 4.4 to see that two terms cancel:

$$
I \propto \sum_{k=0}^{\infty} \frac{\cancel{(-\beta/2)_k}, (n - \beta/2)_k, \left(-m - n + \frac{\alpha - \beta}{2} \right)_k}{(d/2)_k \cancel{(-\beta/2)_k}} \frac{\|\boldsymbol{x}\|_2^{2k}}{k!} ,
$$

which results back in a $_2F_1$ function (two terms in the numerator, one in the denominator), the so-called Gaussian hypergeometric function, cf. Lemma 4.1, and after combining $C_{a,b,n}$, $C_{a,b,n,k}$, $\frac{\pi^{d/2}}{\Gamma(d/2)}$ with the gamma-function expansion of $B\left(\frac{\beta+d}{2}, m - \frac{\alpha+d}{2} + k + 1 \right)$ according to Equation (4.1), and cancelling terms, one finally obtains

$$
I = \frac{\pi^{d/2} \Gamma\left(1 + \frac{\beta}{2}\right) \Gamma\left(\frac{\beta+d}{2}\right) \Gamma\left(m + n - \frac{\alpha+d}{2} + 1\right)}{\Gamma\left(\frac{d}{2}\right) \Gamma(n+1) \Gamma\left(\frac{\beta}{2} - n + 1\right) \Gamma\left(\frac{\beta-\alpha}{2} + m + n + 1\right)} {}_2F_1 \left(\begin{matrix} n - \frac{\beta}{2}, -m - n + \frac{\alpha-\beta}{2} \\ \frac{d}{2} \end{matrix} ; \|\boldsymbol{x}\|_2^2 \right) ,
$$

concluding the proof.   □

Lemma 2.4 from Biler, Imbert and Karch 2011; Magnus et al. 1967 is based on the *Weber-Schafheitlin* integral of two Bessel functions given in Milne-Thomson 1945. The Weber-Schafheitlin integrals are related to the fractional Laplacians of aforementioned functions because the Fourier transform of $_2F_1$ is a Bessel function. For a more generalised version of Lemma 2.4, see Yanghong Huang 2014.

Also note that for even integer β, the prefactor in Theorem 4.3 sometimes contains an expression of the form $\Gamma(-n)$, $n \in \mathbb{N}$ which in principle leads to undefined behaviour (cf. Definition 4.2 together with the property that $k\Gamma(k) = \Gamma(k+1)$). However, one can consider the limit as $x \in \mathbb{R}^+$ approaches an integer n to say that

$$
\lim_{x \to n} \Gamma(-x) = (-1)^{n-1} \infty , \quad \text{or equivalently} \quad \lim_{x \to n} \frac{1}{\Gamma(-x)} = 0 ,
$$

in which case we are lucky because $\Gamma(\beta/2 - n + 1)$ appears in the denominator of the prefactor and without any singularities in the numerator we can safely evaluate the entire expression to 0.

Because $I_{m,n}^{\alpha,\beta}(\boldsymbol{x})$ only depends on the squared radius $r^2 = \|\boldsymbol{x}\|_2^2$, let it also be denoted by $I_{m,n}^{\alpha,\beta}(r^2) = I_{m,n}^{\alpha,\beta}(\boldsymbol{x})$. Further, let

$$\overline{I}_{m,n}^{\alpha,\beta} := \frac{\left\langle x \mapsto I\left(\frac{x+1}{2}\right), P_0^{(a,b)} \right\rangle}{\left\langle P_0^{(a,b)}, P_0^{(a,b)} \right\rangle} = \frac{1}{h_0^{(a,b)}} \int_{-1}^{1} I_{m,n}^{\alpha,\beta}\left(\frac{x+1}{2}\right) w(x)\,\mathrm{d}x\,, \qquad (4.4)$$

denote the 0th coefficient in a Jacobi expansion of $I_{m,n}^{\alpha,\beta}(\boldsymbol{x})$ (recall that $r^2 = \frac{x+1}{2}$ and $P_0^{(a,b)}(x) = 1$) with $h_k := \left\langle P_k^{(a,b)}, P_k^{(a,b)} \right\rangle$ the normalisation coefficients of the basis.

Adding to our collection of tools, in order to solve the problem given in Definition 2.4 we need to normalise the solution by its mass. The normalisation constant is given in Lemma 4.3, based only on a single coefficient ρ_0, allowing for a highly efficient renormalisation.

Lemma 4.3: Mass of the Solution

For a given solution $\rho : B_1(\boldsymbol{0}) \mapsto \mathbb{R}$, its *mass* $M \in \mathbb{R}$ is given by Equation (2.4). Provided the appropriate ansatz given in Equation (4.3), an expansion of weighted radial Jacobi polynomials with coefficients ρ_k, its *mass* is given by

$$M[\rho[\boldsymbol{\rho}]] = \int_{\mathrm{supp}(\rho)} \rho(y)\,\mathrm{d}y = \frac{\pi^{d/2}\Gamma(a+1)}{\Gamma\left(a + d/2 + 1\right)}\,\rho_0\,,$$

so solely depending on the first coefficient ρ_0.

Proof (adapted from Gutleb, José A. Carrillo and S. Olver 2022a). To shorten notation, let $b := \frac{d-2}{2}$. The domain and radial symmetry of our problem suggests the use of hyperspherical coordinates:

$$\begin{aligned}
M = \int_{B_1(\boldsymbol{0})} \rho(\boldsymbol{x})\,\mathrm{d}\boldsymbol{x} &= \sum_{k=0}^{N-1} \rho_k \int_{B_1(\boldsymbol{0})} \left(1 - \|\boldsymbol{x}\|_2^2\right)^a P_k^{(a,b)}(2\|\boldsymbol{x}\|_2^2 - 1)\,\mathrm{d}\boldsymbol{x} \\
&= \sum_{k=0}^{N-1} \rho_k \int_{\partial B_1(\boldsymbol{0})} \mathrm{d}\Omega \int_{r=0}^{1} (1 - r^2)^a P_k^{(a,b)}(2r^2 - 1)r^{d-1}\,\mathrm{d}r \\
&= \Omega_d \sum_{k=0}^{N-1} \rho_k \int_{r=0}^{1} (1 - r^2)^a P_k^{(a,b)}(2r^2 - 1)r^{d-1}\,\mathrm{d}r\,,
\end{aligned}$$

where $\Omega_d = 2\pi^{d/2}/\Gamma(d/2)$ is the surface area of the d-dimensional hypersphere (cf. Lemma 4.4) with radius $R = 1$. Substituting $u := 2r^2 - 1$, therefore $r^2 = \frac{1+u}{2}$ and

$(1 - r^2)^a = \left(\frac{1-u}{2}\right)^a = 2^{-a}(1-u)^a$ as well as $\mathrm{d}r = \frac{\mathrm{d}u}{4r}$,

$$M = 2^{-a}\Omega_d \sum_{k=0}^{N-1} \rho_k \int_{u=-1}^{1} (1-u)^a P_k^{(a,b)}(u) r^{d-1} \frac{\mathrm{d}u}{4r}$$

$$= 2^{-2} 2^{-a}\Omega_d \sum_{k=0}^{N-1} \rho_k \int_{-1}^{1} (1-u)^a P_k^{(a,b)}(u) r^{d-2}\, \mathrm{d}u\,,$$

we notice that $r^{d-2} = \left(\frac{1+u}{2}\right)^{\frac{d-2}{2}} = 2^{-b}(1+u)^b$ and so we have

$$M = 2^{-2} 2^{-a} 2^{-b}\Omega_d \sum_{k=0}^{N-1} \rho_k \int_{-1}^{1} (1-u)^a (1+u)^b P_k^{(a,b)}(u)\, \mathrm{d}u$$

$$= 2^{-(2+a+b)}\Omega_d \sum_{k=0}^{N-1} \rho_k \int_{-1}^{1} (1-u)^a (1+u)^b P_k^{(a,b)}(u) P_0^{(a,b)}(u)\, \mathrm{d}u$$

$$= 2^{1-(2+a+b)} \frac{\pi^{d/2}}{\Gamma(d/2)} \sum_{k=0}^{N-1} \rho_k \frac{2^{a+b+1}\Gamma(a+1)\Gamma(b+1)}{0!(a+b+1)\Gamma(a+b+1)} \delta_{0,k}$$

$$= \frac{\pi^{d/2}\Gamma(a+1)}{\Gamma(a+d/2+1)} \rho_0\,,$$

which relies on the classical orthogonality condition of the Jacobi polynomials given in Theorem 4.2 with the 0th polynomial $P_0(u) = 1$. $\square$

Note that $M = 1$ together with $a > -1$ implies $\rho_0 > 0$ because the factor between both is positive.

Lemma 4.4: Surface Area of the Hypersphere

The surface area of the d-dimensional hypersphere $\partial B_R(\mathbf{0})$ is given by

$$\Omega_d(R) = \frac{\mathrm{d}}{\mathrm{d}R} V_d(R) = \frac{\mathrm{d}}{\mathrm{d}R} \left(\frac{2\pi^{d/2}}{d\Gamma(d/2)} R^d \right) = \frac{2\pi^{d/2}}{\Gamma(d/2)} R^{d-1}\,.$$

Proof. We find Ω_d by evaluation of the d-dimensional Gaussian integral

$$I_d := \int_{\mathbb{R}^d} \mathrm{e}^{-\|\boldsymbol{x}\|_2^2}\, \mathrm{d}\boldsymbol{x} = \int_{\mathbb{R}} \mathrm{d}x_1 ... \int_{\mathbb{R}} \mathrm{d}x_d\, \mathrm{e}^{-x_1^2 - \cdots - x_d^2} = \left(\int_{\mathbb{R}} \mathrm{e}^{-x_1^2}\, \mathrm{d}x_1 \right)^d = (I_1)^d\,,$$

using Fubini's theorem $(I_d < \infty)$. Considering the case $d = 2$, we have

$$I_2 = \int_{\mathbb{R}^2} \mathrm{e}^{-\|\boldsymbol{x}\|_2^2}\, \mathrm{d}\boldsymbol{x} = \int_0^{2\pi} \mathrm{d}\theta \int_0^{\infty} r\mathrm{e}^{-r^2}\, \mathrm{d}r = -2\pi \int_0^{-\infty} \mathrm{e}^u \frac{\mathrm{d}u}{2} = \pi \int_{-\infty}^{0} \mathrm{e}^u\, \mathrm{d}u = \pi\,,$$

taking the classical approach of transitioning to polar coordinates r, θ (with Jacobi determinant r^{d-1} in the d-dimensional case) immediately leading us to $I_1 = \sqrt{\pi}$.

Generalising this to higher dimensions d with hyperspherical coordinates,

$$I_d = \int_{\mathbb{R}^d} \mathrm{e}^{-\|\boldsymbol{x}\|_2^2}\,\mathrm{d}\boldsymbol{x} = \Omega_d \int_0^\infty r^{d-1}\mathrm{e}^{-r^2}\,\mathrm{d}r = \Omega_d \int_0^\infty s^{d/2-1}\mathrm{e}^{-s}\frac{\mathrm{d}s}{2} = \frac{\Omega_d}{2}\Gamma(d/2)\,,$$

where once again $r := \|\boldsymbol{x}\|_2$ and using a substitution $s := r^2$, we must find equality with the above result $I_d = \pi^{d/2}$,

$$I_d = \pi^{d/2} \overset{!}{=} \frac{1}{2}\Omega_d\Gamma(d/2) \quad \Leftrightarrow \quad \Omega_d = \frac{2\pi^{d/2}}{\Gamma(d/2)}\,.$$

Now integrating over the R-ball $B_R(\boldsymbol{0})$, we obtain $V_d(R) := |B_R(\boldsymbol{0})| = \Omega_d \int_0^R r^{d-1}\,\mathrm{d}r = \frac{\mathbb{R}^d\Omega_d}{d}$ and therefore $\Omega_d(R) = \frac{\mathrm{d}V_d(R)}{\mathrm{d}R} = \frac{2\pi^{d/2}}{\Gamma(d/2)}R^{d-1}$. $\qquad\square$

4.4   Derivation of the Operator

Similar to Definition 2.3, we can define the (single) power law operator $\mathcal{Q}^\beta$:

> **Definition 4.8: Power Law Operator $\mathcal{Q}^\beta$**
>
> The power law operator $\mathcal{Q}^\beta : \mathcal{L} \mapsto \mathcal{L}$ is given by
>
> $$\mathcal{Q}^\beta[\rho](\boldsymbol{x}) := \int \|\boldsymbol{x} - \boldsymbol{y}\|_2^\beta \, \mathrm{d}\rho(\boldsymbol{y}) = \int_{\mathrm{supp}(\rho)} \|\boldsymbol{x} - \boldsymbol{y}\|_2^\beta \, \rho(\boldsymbol{y}) \, \mathrm{d}\boldsymbol{y} \,,$$

The operator $\mathcal{Q}^\beta$ acting on an equilibrium measure $\rho(\boldsymbol{x})$ returns the energy $\tilde{E}(\boldsymbol{x}) = \mathcal{Q}^\beta[\rho](\boldsymbol{x})$ at a point $\boldsymbol{x} \in B_1(\boldsymbol{0})$ in our normalised domain. We will start by only considering a single power law operator (out of two in the case of an attractive-repulsive interaction potential $K_{\alpha,\beta}$). Substituting our ansatz given in Equation (4.3) into $\mathcal{Q}^\beta[\rho]$, we obtain

$$\mathcal{Q}^\beta[\rho](x) = \sum_{k=0}^{N-1} \rho_k \int_{B_1(\boldsymbol{0})} \|\boldsymbol{x} - \boldsymbol{y}\|_2^\beta \left(1 - \|\boldsymbol{y}\|_2^2\right)^a P_k^{(a,b)} \left(2 \|\boldsymbol{y}\|_2^2 - 1\right) \, \mathrm{d}\boldsymbol{y} \,, \qquad (4.5)$$

luckily containing the integral evaluated in Theorem 4.3.

We are now interested in a numerical representation of the operator $\mathcal{Q}^\beta$ acting on the function $\rho \in \mathcal{L}$, so an equivalent (linear) operator $Q^\beta : \mathbb{R}^N \mapsto \mathbb{R}^N$ acting on the coefficients $\rho_k \in \mathbb{R}$, $k = 0, ..., N - 1$. As every finite-dimensional linear operator must have a matrix representation, we are looking for a $Q^\beta \in \mathbb{R}^{N \times N}$ such that

$$\mathcal{Q}^\beta[\rho](\boldsymbol{x}) = \boldsymbol{P}^{(a,b)} \left(2 \|\boldsymbol{x}\|_2^2 - 1\right) \cdot Q^\beta \boldsymbol{\rho} \,,$$

where $\boldsymbol{P}^{(a,b)} \left(2 \|\boldsymbol{x}\|_2^2 - 1\right) \in \mathbb{R}^N$ is the vector of radial Jacobi polynomials $P_0^{(a,b)}(x)$, $P_1^{(a,b)}(x)$, ..., $P_{N-1}^{(a,b)}(x)$ evaluated at $2 \|\boldsymbol{x}\|_2^2 - 1$ as introduced in and after Definition 4.6. Note that in the context of linear combinations of Jacobi polynomials, we will use zero-based indexing for vectors and matrices due to the convention that the first orthogonal polynomial is usually denoted by $p_0(x) = 1$, in line with $\deg(p_k) = k$.

Based on the Three-Term Recurrence Relationship (cf. Theorem 4.1), one can even determine an explicit relationship between the coefficients in the Jacobi expansion by considering the Jacobi Matrix (cf. Remark 4.4).

Therefore, starting from Equation (4.5), we obtain

$$\mathcal{Q}^\beta[\rho](\boldsymbol{x}) = \sum_{k=0}^{N-1} \rho_k \mathcal{Q}^\beta[wP_k](\boldsymbol{x}) = \sum_{k=0}^{N-1} \rho_k \sum_{j=0}^{N-1} q_{kj} P_k^{(a,b)} \left(2\left\|\boldsymbol{x}\right\|_2^2 - 1\right)$$

$$= \sum_{j=0}^{N-1}\sum_{k=0}^{N-1} \rho_k q_{kj} P_k^{(a,b)} \left(2\left\|\boldsymbol{x}\right\|_2^2 - 1\right) ,$$

which we will rewrite in matrix-form,

$$\mathcal{Q}^\beta[\rho](\boldsymbol{x}) = \boldsymbol{P}(\boldsymbol{x}) \cdot \begin{pmatrix} \sum_{k=0}^{N-1} \rho_k q_{k,1} \\ \vdots \\ \sum_{k=0}^{N-1} \rho_k q_{k,N} \end{pmatrix} = \boldsymbol{P}(\boldsymbol{x}) \cdot \underbrace{\begin{pmatrix} q_{00} & \cdots & q_{0,N-1} \\ \vdots & \ddots & \vdots \\ q_{N-1,0} & \cdots & q_{N-1,N-1} \end{pmatrix}}_{=:Q^\beta} \begin{pmatrix} \rho_0 \\ \vdots \\ \rho_{N-1} \end{pmatrix}$$

$$= \boldsymbol{P}^{(a,b)} \left(2\left\|\boldsymbol{x}\right\|_2^2 - 1\right) \cdot Q^\beta \boldsymbol{\rho}$$

where we used $\boldsymbol{P}(\boldsymbol{x}) = \boldsymbol{P}^{(a,b)}\left(2\left\|\boldsymbol{x}\right\|_2^2 - 1\right)$ as a shorthand giving us the form of the operator matrix. Its first row, the set of coefficients for the constant Jacobi polynomial $P_0^{(a,b)}$ of each expansion of the Q operator, weighted by the solution coefficients, adds up to the total energy E (coefficient of the constant polynomial). All remaining rows of Q contain coefficients for polynomials of degree at least 1, so their weighted contributions must add up to 0 in order for the total energy $\tilde{E}(\boldsymbol{x})$ to remain constant.

For the attractive-repulsive interaction potential $K_{\alpha,\beta}$, because each column consists of an expansion of the Jacobi polynomials, we have $q_{0k} = I_{m,k}^{\alpha,\beta}$.
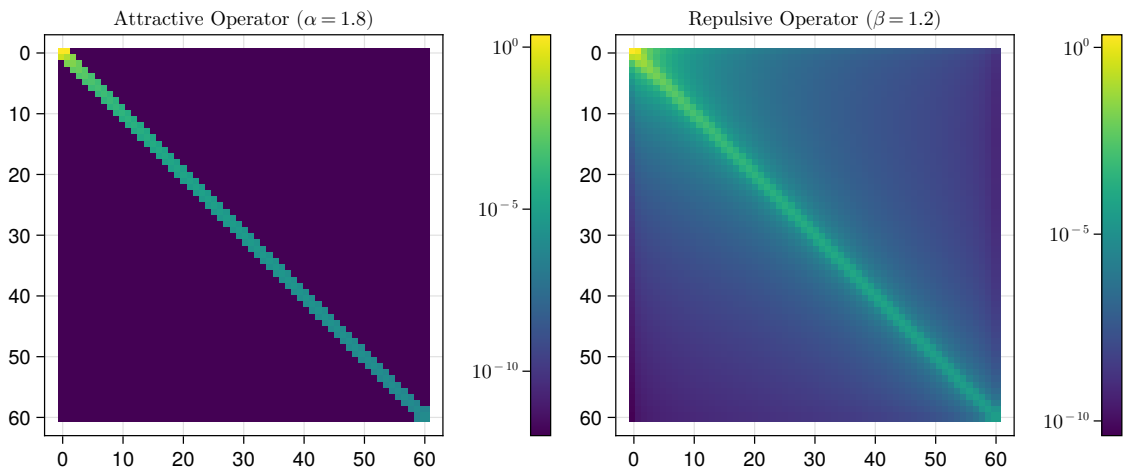
Figure 4.2: The attractive and repulsive operators (matrices) as given in Definition 4.8, the matrix values are shown in a $\log_{10}$ colour scale. Due to the choice of basis, the attractive operator is exactly banded. The repulsive parameter is only approximately banded, which the spy plots effectively demonstrate.

The bandedness of the attractive operator in Figure 4.2 is due to the three-term recurrence relationship of the Jacobi polynomial basis (cf. Theorem 4.1 and Definition 4.6). For the attractive-repulsive interaction potential $K_{\alpha,\beta}(r)$, the full operator is given by

$$
\begin{aligned}
\mathcal{Q}_{\alpha,\beta}[\hat{\rho}](\hat{\boldsymbol{x}}) &:= \int_{B_R(\boldsymbol{0})} K_{\alpha,\beta}\left(\|\hat{\boldsymbol{x}} - \hat{\boldsymbol{y}}\|_2\right) \hat{\rho}(\hat{\boldsymbol{y}}) \,\mathrm{d}\hat{\boldsymbol{y}} \\
&= \int_{B_R(\boldsymbol{0})} \left(\frac{\|\hat{\boldsymbol{x}} - \hat{\boldsymbol{y}}\|_2^\alpha}{\alpha} - \frac{\|\hat{\boldsymbol{x}} - \hat{\boldsymbol{y}}\|_2^\beta}{\beta} \right) \hat{\rho}(\hat{\boldsymbol{y}}) \,\mathrm{d}\hat{\boldsymbol{y}} \\
&= \int_{B_1(\boldsymbol{0})} \left(\frac{R^\alpha \|\boldsymbol{x} - \boldsymbol{y}\|_2^\alpha}{\alpha} - \frac{R^\beta \|\boldsymbol{x} - \boldsymbol{y}\|_2^\beta}{\beta} \right) \hat{\rho}(R\boldsymbol{y}) \, R^d \mathrm{d}\boldsymbol{y} \\
&= R^d \int_{B_1(\boldsymbol{0})} \left(\frac{R^\alpha}{\alpha} \|\boldsymbol{x} - \boldsymbol{y}\|_2^\alpha - \frac{R^\beta}{\beta} \|\boldsymbol{x} - \boldsymbol{y}\|_2^\beta \right) \rho(\boldsymbol{y}) \,\mathrm{d}\boldsymbol{y} \\
&= \frac{R^{\alpha+d}}{\alpha} \mathcal{Q}^\alpha[\rho](\boldsymbol{x}) - \frac{R^{\beta+d}}{\beta} \mathcal{Q}^\beta[\rho](\boldsymbol{x}) \,,
\end{aligned}
$$

where one needs to carefully handle the variable transform with $\mathrm{d}\hat{\boldsymbol{y}} = R^d \mathrm{d}\boldsymbol{y}$ in d dimensions whereas the vectors themselves obey $\hat{\boldsymbol{y}} = R\boldsymbol{y}$ as established previously. In matrix form that is,

$$
Q_{\alpha,\beta} := \frac{R^{\alpha+d}}{\alpha} Q^\alpha - \frac{R^{\beta+d}}{\beta} Q^\beta \,, \tag{4.6}
$$

for some interval radius $R \in \mathbb{R}^+$, usually chosen as the smallest possible R such that $\mathrm{supp}(\rho) \subseteq [-R, R]$.
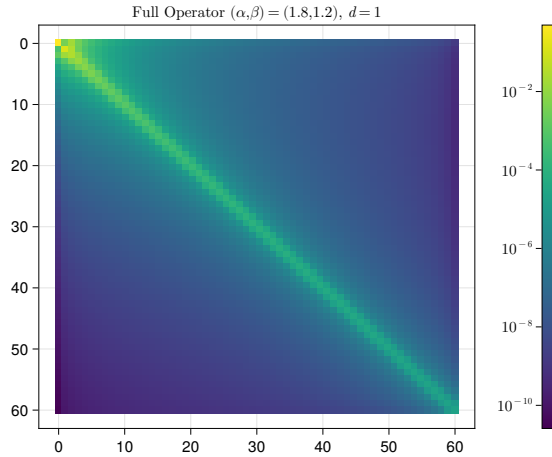
Figure 4.3: Spy plot of $Q_{\alpha,\beta}$, the combination of the attractive-repulsive operators. Inverting this operator and applying it to $(1, 0, ..., 0)^T \in \mathbb{R}^N$ will yield the unnormalised coefficients ρ_k of the solution expansion given in Equation (4.3).

4.5   Solving a Linear System

Once the operator is computed, we are now looking for a set of solution coefficients $\boldsymbol{\rho} \in \mathbb{R}^N$ such that the total energy $E = E_{\text{kin}} + U = U = U_K[\hat{\rho}]$ (in the presence of friction, the kinetic energy will eventually dissipate, cf. Chapter 2) on the domain $D = B_R(\mathbf{0})$ is constant. That means, we are looking for $\boldsymbol{\rho} \in \mathbb{R}^N$ such that

$$\mathcal{Q}[\rho](\boldsymbol{x}) = \tilde{E}(\boldsymbol{x}) = E \,, \tag{4.7}$$

where we can expand $\tilde{E}(\boldsymbol{x}) = \boldsymbol{P}^{(a,b)}\left(2\left\|\boldsymbol{x}\right\|_2^2 - 1\right) \cdot \boldsymbol{E}$ into Jacobi polynomials with coefficients $\boldsymbol{E} = E\boldsymbol{e}_1 = (E, 0, ..., 0)^T$ such that the energy is constant along the entire domain, so $\tilde{E}(\boldsymbol{x}) = E \cdot P_0^{(a,b)}\left(2\left\|\boldsymbol{x}\right\|_2^2 - 1\right) = E$. In matrix form, that is

$$Q\boldsymbol{\rho} = \boldsymbol{E} \quad \Leftrightarrow \quad \begin{pmatrix} q_{00} & \cdots & q_{0,N-1} \\ \vdots & \ddots & \vdots \\ q_{N-1,0} & \cdots & q_{N-1,N-1} \end{pmatrix} \begin{pmatrix} \rho_0 \\ \vdots \\ \rho_{N-1} \end{pmatrix} = \begin{pmatrix} E \\ \mathbf{0} \\ 0 \end{pmatrix} \,.$$

This equation $Q\boldsymbol{\rho} = \boldsymbol{E}$ contains two unknowns, so we need a second equation to find the full solution $\rho \in \mathcal{L}$ and, thereby, $\hat{\rho} \in \hat{\mathcal{L}}$. The second piece of information we are looking for is the mass given in Equation (2.4), which is set to $M = 1$. We start by dividing $Q\boldsymbol{\rho} = E\boldsymbol{e}_1$ by the unknown energy E,

$$Q\frac{\boldsymbol{\rho}}{E} = Q\tilde{\boldsymbol{\rho}} = \boldsymbol{e}_1 \,,$$

which we can efficiently solve using readily available linear system solvers. After solving, we ensure $M\left[\rho[\tilde{\boldsymbol{\rho}}]\right] = 1$, using Lemma 4.3, leading us to our final equilibrium distribution $\rho \in \mathcal{L}$.

Hence the total potential (energy) of a given solution $\boldsymbol{\rho}$ is obtained by

$$E(R) = \{Q_{\alpha,\beta}\boldsymbol{\rho}\}_1 = \sum_{k=0}^{N-1} \rho_k \left(\frac{R^{\alpha+d}}{\alpha}\overline{I}_{m,k}^{\alpha,\alpha} - \frac{R^{\beta+d}}{\beta}\overline{I}_{m,k}^{\alpha,\beta}\right) \,, \tag{4.8}$$

with $\overline{I}_{m,n}^{\alpha,\alpha}$ the 0th coefficient of a Jacobi polynomial expansion of $I_{m,n}^{\alpha,\alpha}(\boldsymbol{x})$ (cf. Theorem 4.3) as given in Equation (4.4).

4.5.1   Tikhonov Regularisation

The normal system is: ...

Also referred to as Ridge regression

4.6   Results
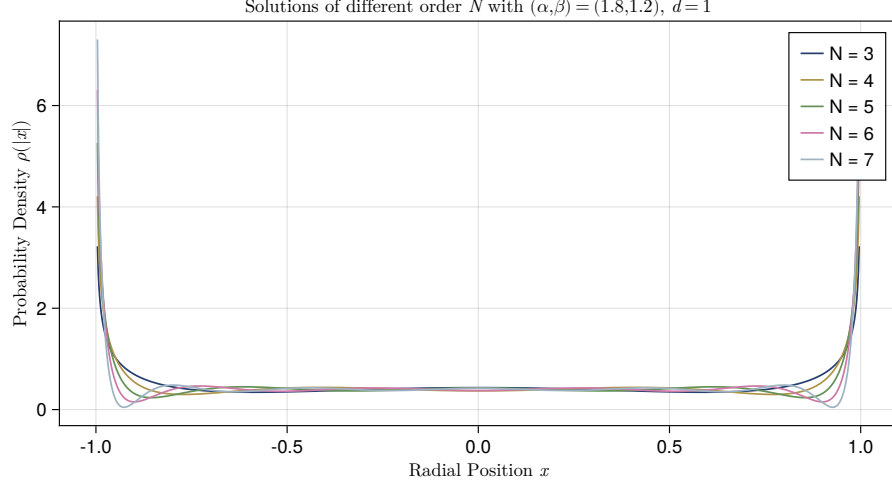
Figure 4.4: Particle density distribution function solutions ρ of increasing order N to the attractive-repulsive problem with interaction potential $K_{alpha,\beta}(r)$, $\alpha = 2.5$ and $\beta = 1.2$. Reflected along the y-axis for better visibility of the domain.

4.7   Outer Optimisation Routine

The unconstrained outer optimisation over the scalar value $R \in \mathbb{R}^+$, the radius of our domain $B_R(\mathbf{0})$, is carried out using Optim.jl's implementation (Mogensen et al. 2023) of the Limited-memory Broyden-Fletcher-Goldfarb-Shanno (LBFGS) optimisation method (Liu and Nocedal 1989), an extension of BFGS for low-memory usage, using an estimate for the gradient based on Automatic Differentiation (AD) techniques.

As part of a comparison between multiple optimisation approaches, LBFGS outperformed the Nelder-Mead and Newton trust region methods for our case, converging extremely quickly within only 3 iterations, 10 function calls and 10 evaluations of the gradient. While the downhill simplex method by Nelder and Mead did not converge to the desired local minimum (cf. Figure 4.5), the trust region method using Newton's method to solve a quadratic model for each subproblem (Sorensen 1982) also converged in only 3 iterations with only 4 function, gradient and Hessian evaluations. Again, the values of the gradient and Hessian (in the case of a one-dimensional optimisation, simply the first and second derivatives), are obtained using AD.

The LBFGS method converged with $\|\nabla E(R)\|_2 \approx 10^{-11}$ while the Newton trust region method converged at $\|\nabla E(R)\|_2 \approx 10^{-9}$. The entire optimisation routine with LBFGS,

including function and gradient evaluations (solving a 12×12 linear system), takes (28 ± 4) ms on an Intel® i7-5600U CPU running at 2.6 GHz.
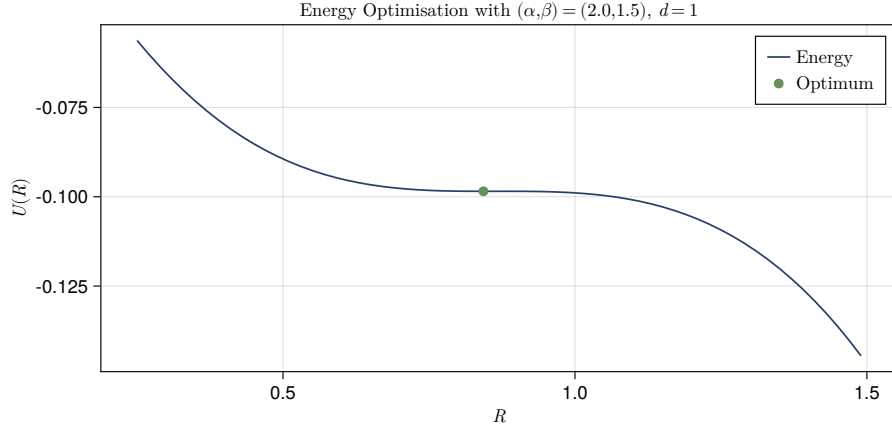
Figure 4.5: The total potential U as a function of the support radius R. This is the goal function minimised by the outer optimisation routine.

Note that using this setup, the operators themselves do not need to be recomputed upon a change in R, cf. Equation (4.6). The provided implementation uses Least Recently Used (LRU) caching to automatically store operators for a given parameter set and order N.

Lemma 4.5: Unique Energy Minimum

Assuming an $N = 1$ expansion of the density distribution ρ according to Equation (4.3) with $m \in \mathbb{N}_0$, for a feasible attractive-repulsive interaction potential $K_{\alpha,\beta}(r) = \frac{r^\alpha}{\alpha} - \frac{r^\beta}{\beta}$ with $\alpha > \beta$ and $\alpha > 0$, the energy minimum $E_{\min} = E(R_{\min})$ is unique and given by

$$R_{\min} = \left(\frac{\alpha(\beta + d)\overline{I}_{m,0}^{\alpha,\beta}}{\beta(\alpha + d)\overline{I}_{m,0}^{\alpha,\alpha}} \right)^{\frac{1}{\alpha - \beta}},$$

with $\overline{I}_{m,n}^{\alpha,\alpha}$ as given in Equation (4.4).

Proof. Starting from the total energy given in Equation (4.8), we obtain the first derivative as

$$\frac{\partial E}{\partial R} = \frac{\partial}{\partial R} \rho_0 \left(\frac{R^{\alpha+d}}{\alpha} \overline{I}_{m,k}^{\alpha,\alpha} - \frac{R^{\beta+d}}{\beta} \overline{I}_{m,k}^{\alpha,\beta} \right) = \rho_0 \frac{\alpha+d}{\alpha} R^{\alpha+d-1} \overline{I}_{m,k}^{\alpha,\alpha} - \rho_0 \frac{\beta+d}{\beta} R^{\beta+d-1} \overline{I}_{m,k}^{\alpha,\beta},$$

---

as $\frac{\partial \rho_0}{\partial R} = 0$ for $N = 1$. Setting the derivative to 0 to find the extremata,

$$\frac{\partial E}{\partial R} = 0 \quad \Leftrightarrow \quad \frac{\alpha + d}{\alpha} R^\alpha \overline{I}_{m,k}^{\alpha,\alpha} = \frac{\beta + d}{\beta} R^\beta \overline{I}_{m,k}^{\alpha,\beta} \quad \Leftrightarrow \quad R^{\alpha-\beta} = \frac{\alpha(\beta + d)}{\beta(\alpha + d)} \frac{\overline{I}_{m,k}^{\alpha,\beta}}{\overline{I}_{m,k}^{\alpha,\alpha}} \,,$$

we obtain a unique extremum $R_{\min} := \left(\frac{\alpha(\beta+d)\overline{I}_{m,0}^{\alpha,\beta}}{\beta(\alpha+d)\overline{I}_{m,0}^{\alpha,\alpha}} \right)^{\frac{1}{\alpha-\beta}}$. Because we must have $\alpha > \beta$ for any stable solution, $\lim_{r\to\infty} K_{\alpha,\beta}(r) = \infty$ and more importantly,

$$\lim_{R\to\infty} E(R) = \lim_{R\to\infty} \rho_0 R^d \left(\frac{R^\alpha}{\alpha} \overline{I}_{m,k}^{\alpha,\alpha} - \frac{R^\beta}{\beta} \overline{I}_{m,k}^{\alpha,\beta} \right) = \infty \,,$$

since both $\overline{I}_{m,k}^{\alpha,\alpha}, \overline{I}_{m,k}^{\alpha,\beta} < \infty$, $\alpha > 0$ and $M > 0 \Rightarrow \rho_0 > 0$, telling us that any $R_{\min} > 0$ must be a minimum between the endpoints $R = 0$ and $R = \infty$. $\qquad \square$

There is strong numerical evidence that the energy minimum is also unique for $N > 1$. Despite significant effort, this remains difficult to prove [1]. Even for $N = 2$, attempting a direct substitution of $\boldsymbol{\rho}$ through the explicit inversion of a 2×2 matrix, leads to finding the roots of a quintic polynomial for which it is well-known that no explicit formula exists.

While the exact value of $R_{\min}$ in Lemma 4.5 is not particularly useful in most scenarios as it only holds for $N = 1$, it provides a solid initial guess for the optimisation routine. Further, $R_{\min} > 0$ is an approximate (necessary) condition for the existence of an energy minimum of a given combination of α and β.

4.8 Comparison with Analytic Solutions

As introduced in Section 2.8, there are some analytical solutions available which allow us to perform further analysis of the numerical method in these special cases.

---

[1]Naming "numerical evidence" is a current topic of discussion in the numerical analysis community
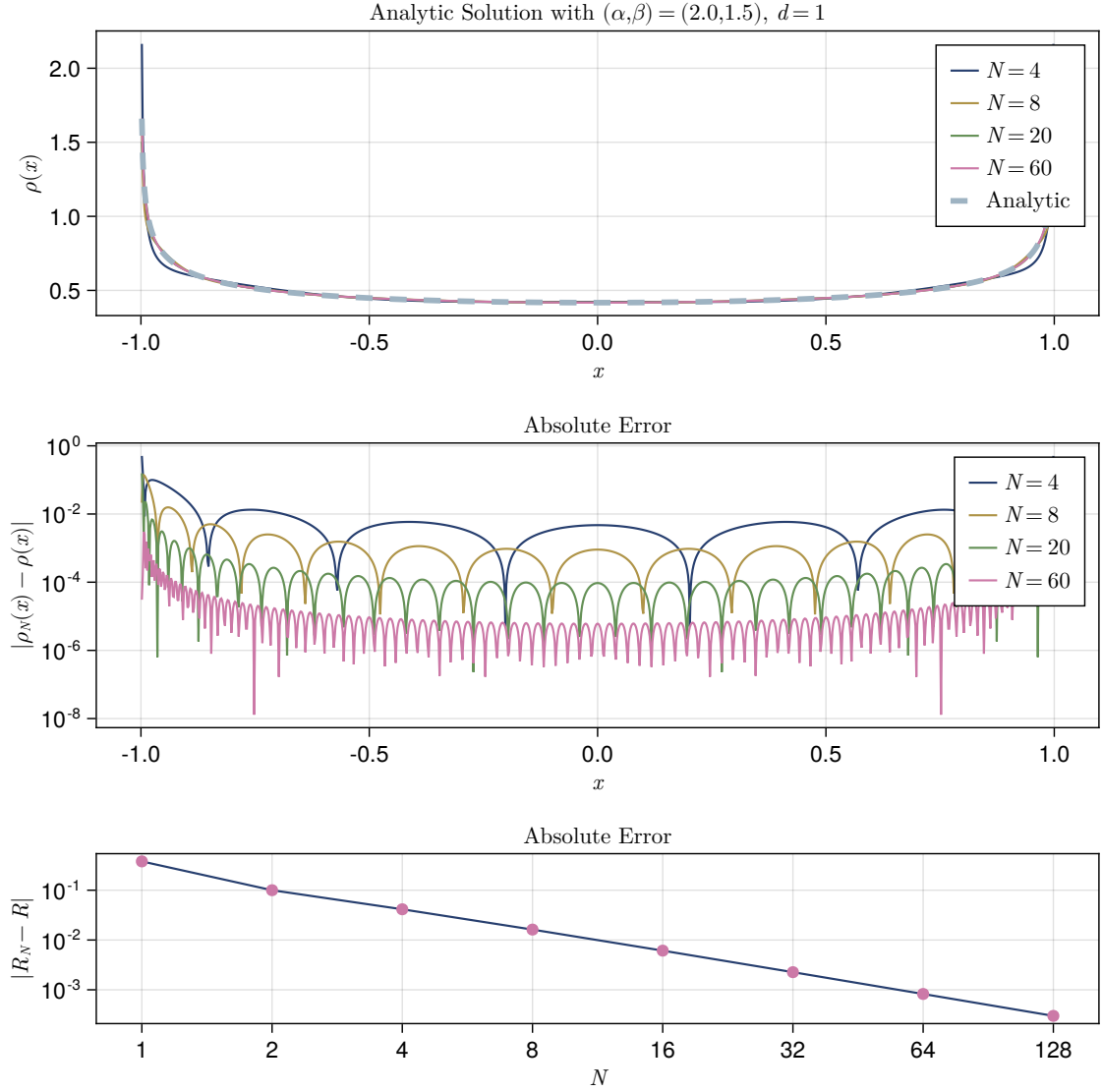
Figure 4.6: The analytic solution $\rho(x)$ given in Equation (2.7) compared to the (spectral method) solutions of different order N. The "arches" occur as a result of the roots of $\rho(x) - \rho_N(x)$, their number approximately equals the order N (a polynomial of degree N has at most N roots).

The reason for this fast convergence is the choice of weighted basis in Equation (4.3) compared to the form of the analytical solution in Equation (2.7). There are more analytic solutions available for other parameter ranges, which we will not analyse within the scope of this dissertation.

> **Definition 4.9: Spectral Convergence**
>
> **Definition 3.6** (Convergence at spectral speed) An N-point approximation φ_N of a function f converges to f at spectral speed if $|\varphi_N - f|$ decays pointwise in $[-1, 1]$ faster than $O(N^{-p})$ for any $p = 1, 2, \ldots$ so $p \in \mathbb{N}$.
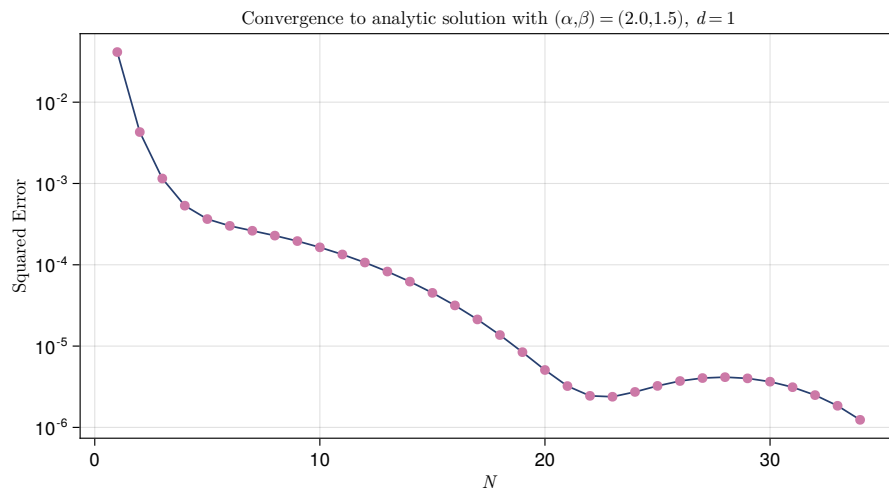
Figure 4.7: Convergence of the numerical solution to the known analytic solution (cf. Equation (2.7)) in a special case where it is known, squared error plotted as a function of the highest order in the expansion N.

4.9   Discussion
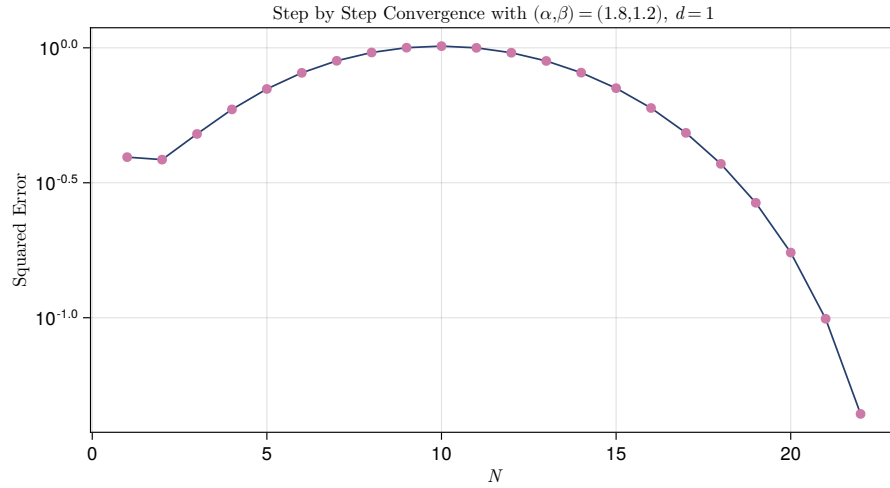
Figure 4.8: Step-by-step convergence of numerical solutions $\rho_N(x)$ as compared to $\rho_{24}(x)$, visualised using the squared error of the pointwise evaluation of both functions in 200 points.
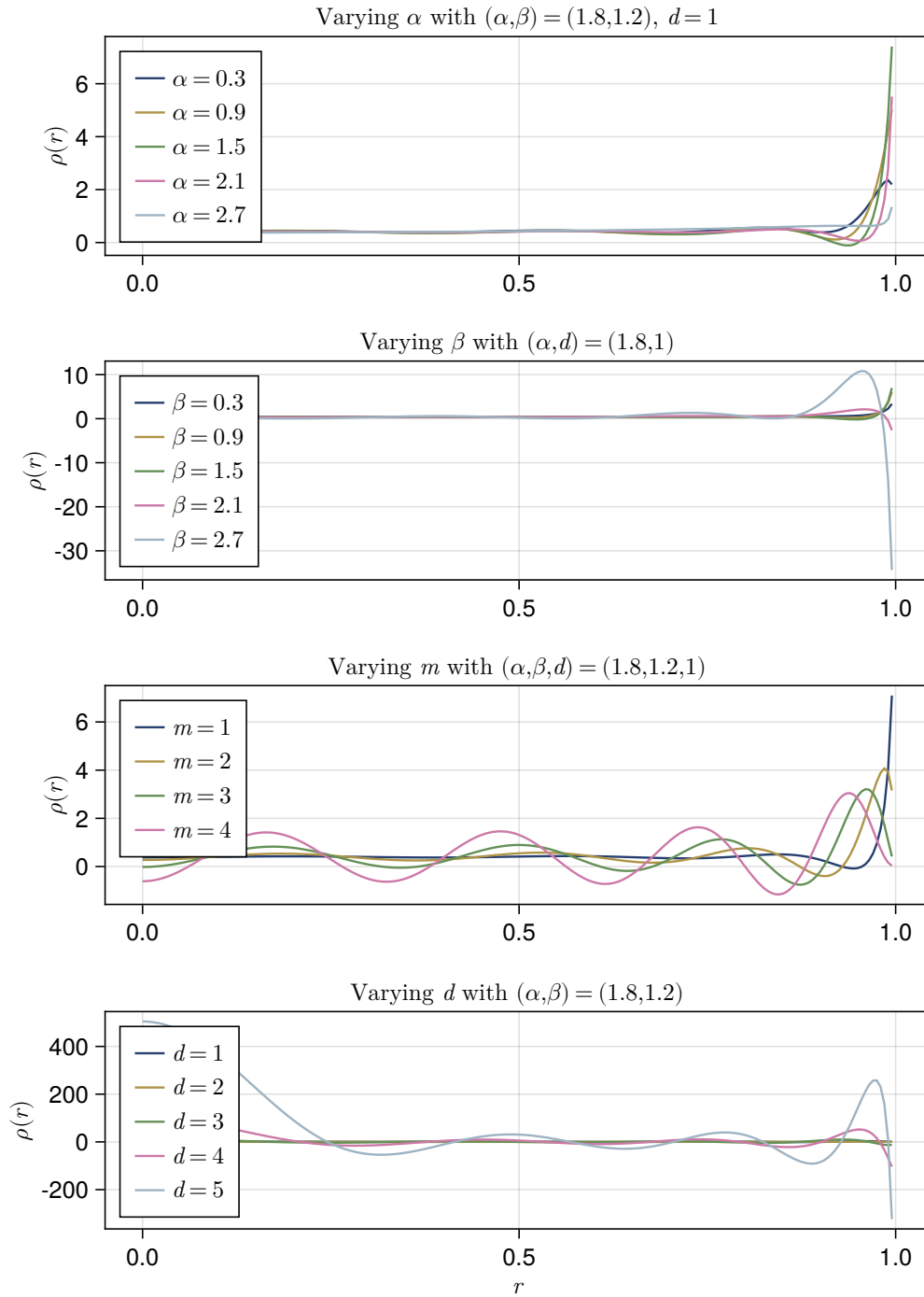
Figure 4.9: Varying different parameters in the solver to demonstrate their effect. See also, Figure 5.5.

Chapter 5

General Kernel Spectral Method

Now that we know how to treat power law potentials in the construction of a spectral method for the solution of equilibrium measures, can we consider more general kernels as well? The approach in this chapter will be to expand a general kernel K in a power law basis and utilise the methodology introduced in the previous chapter to construct a general kernel spectral method.

More specifically, one choice of basis that could be made is the basis of monomials (so integer powers of the power law kernel basis). Using standard methods from function approximation theory, we expand the general kernel $K : \mathbb{R}^+ \mapsto \mathbb{R}$ in the basis of G Jacobi polynomials (cf. Definition 4.6)

$$K(r) \approx \sum_{l=0}^{G-1} \tilde{g}_k P_k^{(a,b)} \left(2r^2 - 1 \right) , \quad \tilde{g}_k \in \mathbb{R},\ l = 0, ..., G - 1 \,,$$

which we then reproject into the monomial basis to obtain the monomial coefficients $g_k \in \mathbb{R}$ such that

$$K_G(r) = \sum_{l=0}^{G-1} g_k r^l \approx K(r), \quad g_k \in \mathbb{R},\ l = 0, ..., G - 1 \,. \tag{5.1}$$

5.1 Reprojection from radial Jacobi polynomials

For versatility in the choice of basis, we obtain the monomial coefficients of a given kernel $K(r)$ by

$$\boldsymbol{g} = B\tilde{\boldsymbol{g}} \,,$$

where $B \in \mathbb{R}^{G \times G}$.

5.2   Description of the Method

Given the Ansatz, the total energy of the equilibrium measure (cf. Definition 2.1) is given by

$$U_{K_G}[\hat{\rho}] = \iint K_G\left(\|\hat{\boldsymbol{x}} - \hat{\boldsymbol{y}}\|_2\right) \mathrm{d}\hat{\rho}(\hat{\boldsymbol{x}})\mathrm{d}\hat{\rho}(\hat{\boldsymbol{y}}) = \sum_{l=0}^{G-1} g_l \iint \|\hat{\boldsymbol{x}} - \hat{\boldsymbol{y}}\|_2^l \, \mathrm{d}\hat{\rho}(\hat{\boldsymbol{x}})\mathrm{d}\hat{\rho}(\hat{\boldsymbol{y}})$$

$$= R^{2d} \sum_{l=0}^{G-1} g_l R^l \iint \|\boldsymbol{x} - \boldsymbol{y}\|_2^l \, \mathrm{d}\rho(\boldsymbol{x})\mathrm{d}\rho(\boldsymbol{y}) = R^{2d} \sum_{l=0}^{G-1} g_l R^l U^{(l)}[\rho] \,,$$

using Definition 2.3.
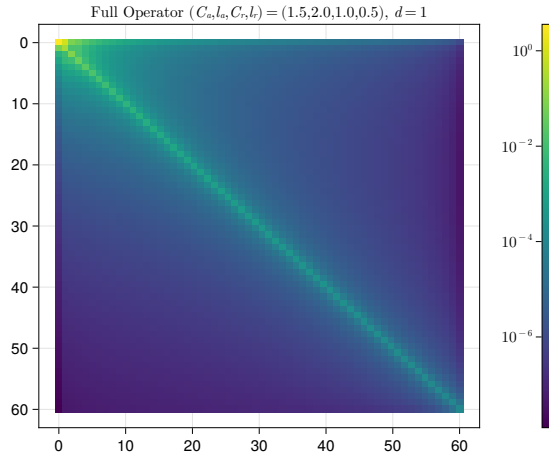
Figure 5.1: The full operator constructed from the $G = 8$th order monomial expansion K_G of the Morse potential function $K_{C_a,l_a,C_r,l_r}(r)$ with parameters as given above.
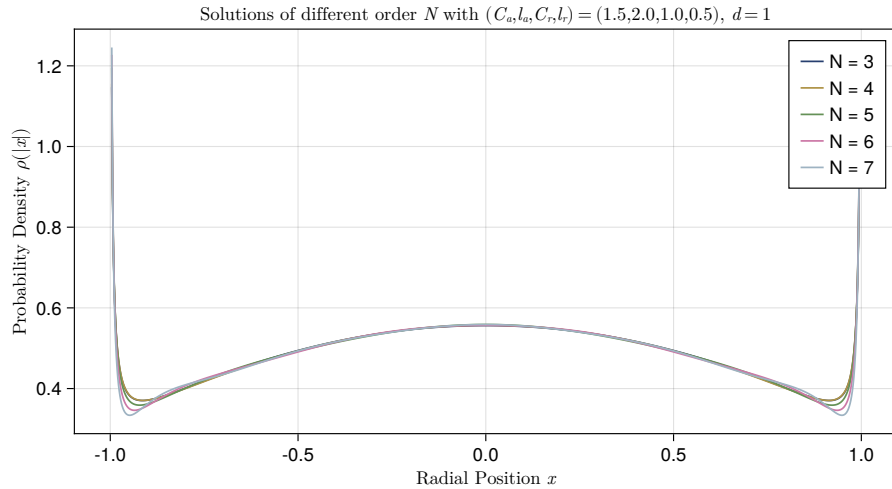
Figure 5.2: Solutions $\rho_N(x)$ of increasing order N in the general kernel setting with a monomial expansion of highest order $G = 8$ of the Morse potential $K_{C_a,l_a,C_r,l_r}(r)$.
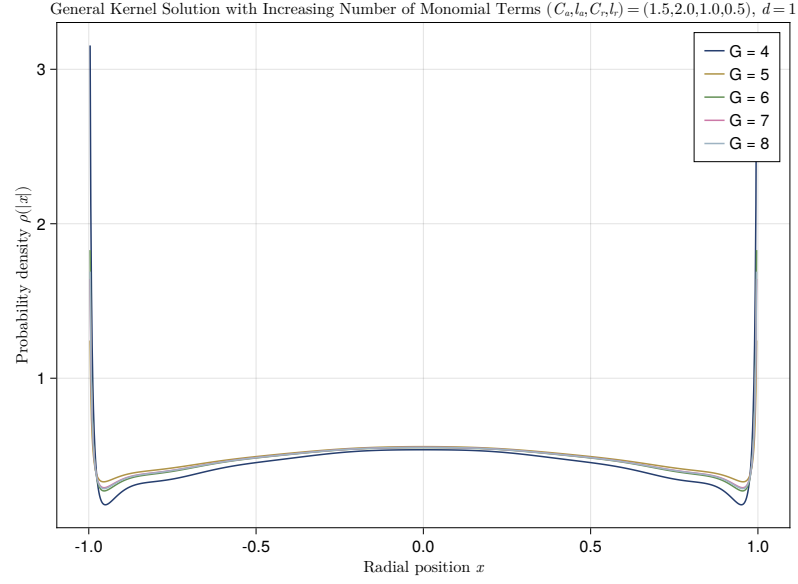
Figure 5.3: Solutions $\rho_8(x)$ for an increasing number of terms G in the monomial expansion of a general kernel K, in this case given by the Morse potential $K_{C_a,l_a,C_r,l_r}(r)$. So each solution $\rho_8(x)$ is a linear combination of 8 Jacobi polynomials together with a weight, cf. Equation (4.3).

As one can see, the solutions improve the better the approximation of the general kernel K becomes with growing order G of its monomial expansion. To make a better statement about this numerical behaviour, consider Figure 5.4.
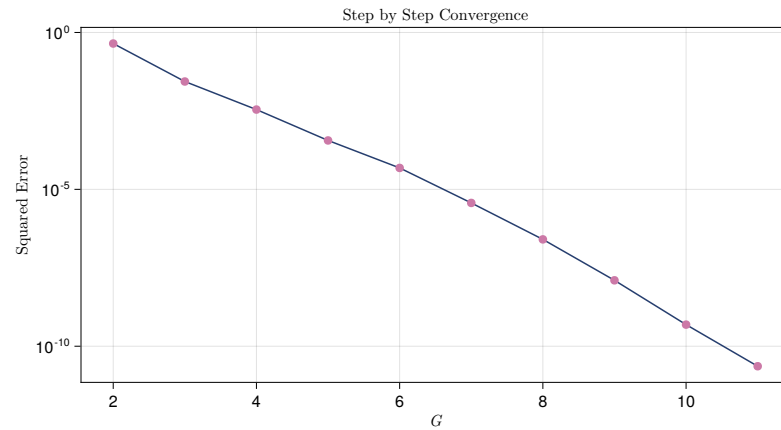
Figure 5.4: Convergence of numerical solutions $\rho_N(x)$ as compared to $\rho_{24}(x)$, visualised using the squared error of the pointwise evaluation of both functions in 200 points. The solver again uses $K(r) = K_{C_a,l_a,C_r,l_r}(r)$.
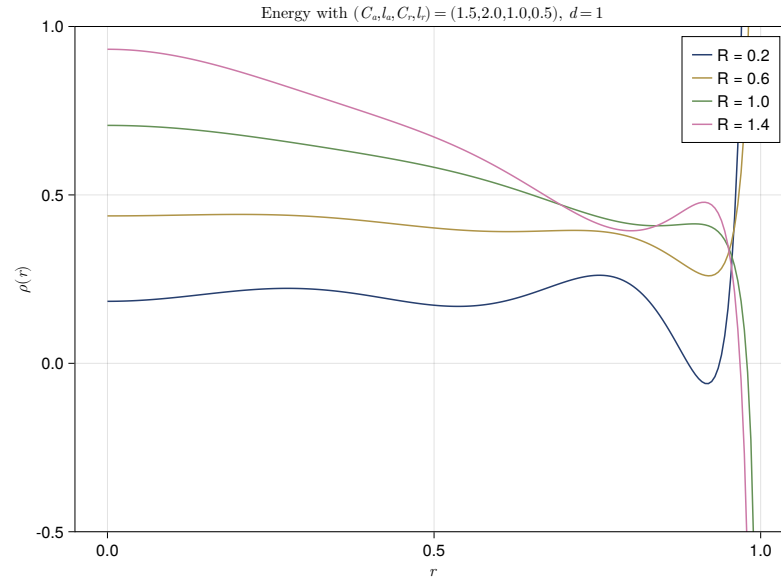
Figure 5.5: General kernel solutions ($N = 6$, $G = 8$) with varying R when using the Morse potential $K_{C_a,l_a,C_r,l_r}(r)$ with parameters as given above.

Chapter 6

Implementation and Results
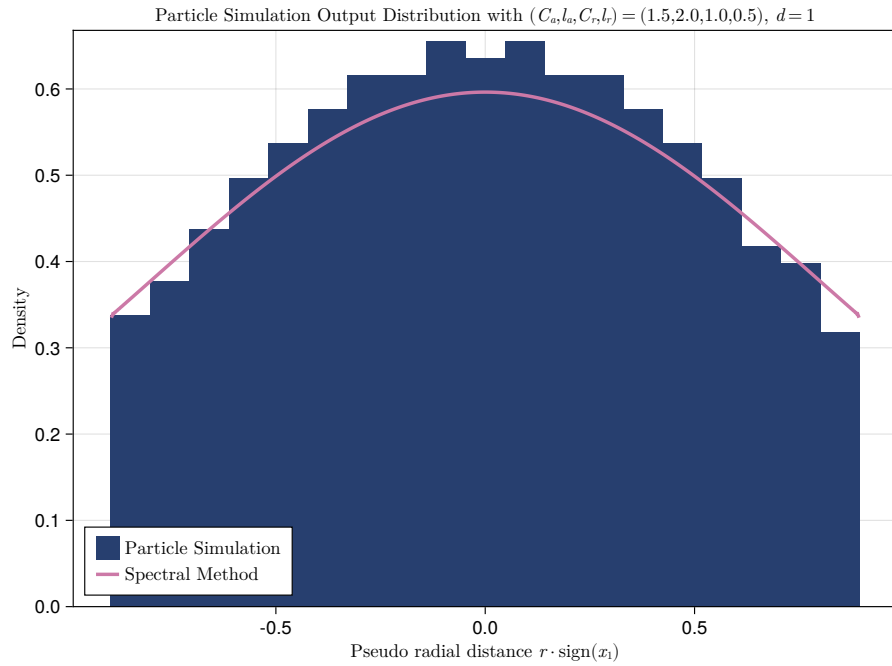
Figure 6.1: Comparison of the radial distance histogram from the simulation output with the $G = 8$ general kernel solvers' equilibrium measure $\rho_{12}(r)$ at R given by the simulator, so without using the outer optimisation routine. The interaction potential in this example is $K(r) = K_{C_a, l_a, C_r, l_r}(r)$ with parameters given above.

6.1   Further Discussion

6.1.1   Well-Conditionedness

A common flaw of spectral collocation methods, one could think of them as the highest-order limit of finite difference schemes, is their bad conditioning behaviour.

Ideally, we would like the condition number $\kappa(Q)$ to be independent of the order N to which we solve our problem. That means we want

$$\kappa(Q) := \frac{\sigma_{\max}(Q)}{\sigma_{\min}(Q)} = \frac{\|Q\|_2}{\|Q^{-1}\|_2} = \mathcal{O}(1)$$

and not $\mathcal{O}(N)$ or even higher orders.
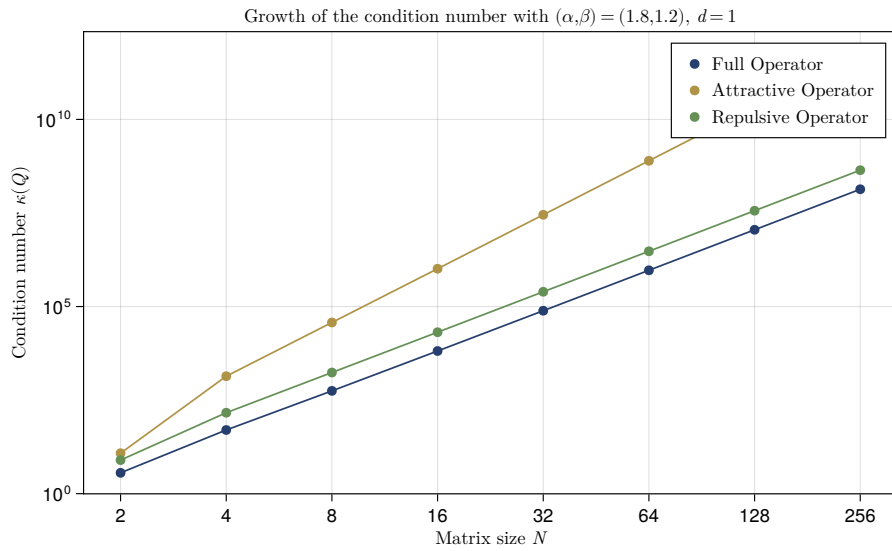
Figure 6.2: Growth of the 2-norm condition number $\kappa(Q)$ of the attractive-repulsive operator Q.
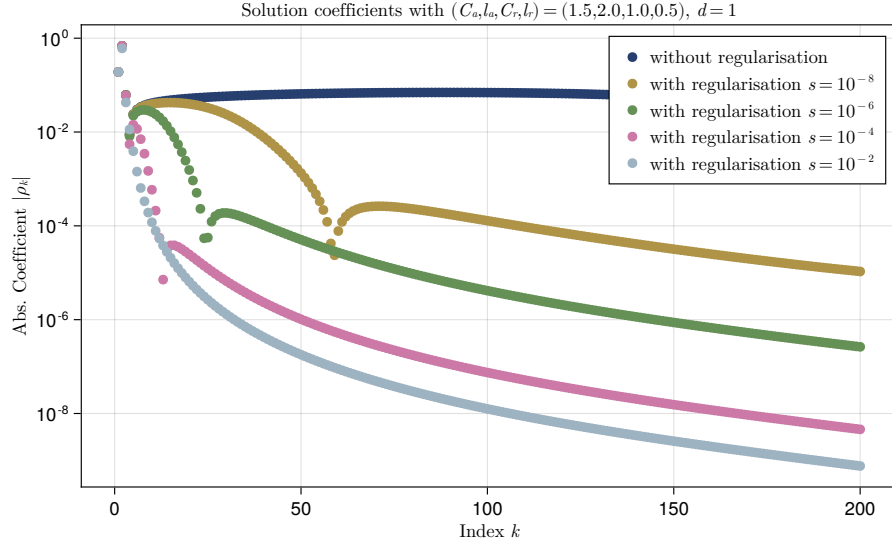
Figure 6.3: Absolute value of the solution coefficients ρ_k with and without Tikhonov regularisation.

6.2 Implementation Architecture

The spectral method solver is written in Julia (Bezanson et al. 2017) whereas the simulator is written in C++.

To compile the simulator, please run

```
$ conan install .  --output-folder=build --build=missing
$ cd build; cmake ..  -DCMAKE_BUILD_TYPE=Release
$ make -j4 in a bash terminal.
```

In order to run tests of the numerical solver implementation, run

```
$ julia solver/tests.jl
```

in a bash terminal. In order to regenerate all plots at once, including simulation output from the C++ implementation, run

```
$ julia solver/plotall.jl in a terminal.
```

To be done / included.

6.3 Runtime Analysis

The following benchmarks were accumulated on an Intel® i7-5600U CPU running at 2.6 GHz as the average over 3 individual runs with different test vectors, consistent across different parameter runs.

To be done / included.

Chapter 7

Conclusion

Here we summarise the work that has been presented in this dissertation and discuss possible areas for future work.

7.1 Summary

In the present thesis, we explored the surprisingly complex behaviour of many body systems arising from simple pairwise particle-particle interactions and, in some cases, self-propulsion and friction terms. For certain types of interactions, these systems approach equilibrium distributions $\rho(\boldsymbol{x})$ which we aim to solve for using a spectral method, assuming their radial symmetry (a natural supposition in the absence of an external potential).

After introducing some theory in Chapter 2 and setting up a particle simulator to verify our findings in Chapter 3, we constructed a spectral method for power law interaction potentials in Chapter 4 based on Jacobi polynomials. The resulting spectral method is a highly efficient direct method with excellent convergence properties and solvability due to the banded operators appearing in it. As an original extension, we introduced a numerical method for constructing the spectral solution for general kernels $K(r)$ in Chapter 5. Both methods reproduce analytical solutions to arbitrary precision and provide solutions for cases in which analytical solutions are unknown. We finally compared the numerical solution in the continuous situation with particle simulations in Chapter 6.

Next to the written part, the reader will find an implementation of the particle simulator written in C++ online (Waldert 2023), including a GUI, as well as the spectral method solver written in Julia.

7.2   Future Work

Other approaches, such as the one in Wu et al. 2015 show that ...

<div align="center">**To be done / included.**</div>

7.3   Conclusion

This method is exponentially faster than previous techniques, requiring only minutes or seconds instead of days. Importantly, the detection time is not influenced by the system's complexity—a solution to the long-standing scalability challenge.

Acronyms, Definitions and Theorems

AD	Automatic Differentiation	37
fcc	face-centered cubic	17
FMM	Fast Multipole Method	13
GUI	Graphical User Interface	12
LBFGS	Limited-memory Broyden-Fletcher-Goldfarb-Shanno	37
LRU	Least Recently Used	38
PDE	Partial Differential Equation	2

Definitions

Theorems

Lemmata

Remarks

Bibliography

Akita, Kiyomi and Fumitake Yoshida (Jan. 1973). 'Gas Holdup and Volumetric Mass Transfer Coefficient in Bubble Columns. Effects of Liquid Properties'. In: *Ind. Eng. Chem. Process Des. Dev.* 12.1, pp. 76–80. ISSN: 0196-4305. DOI: `10.1021/i260045a015`.

Arora, Manmohan S. and S. D. Bajpai (Jan. 1995). 'A new proof of the orthogonality of Jacobi polynomials'. In: *Demonstratio Math.* 28.1, pp. 177–180. ISSN: 2391-4661. DOI: `10.1515/dema-1995-0122`.

Bezanson, Jeff, Alan Edelman, Stefan Karpinski and Viral B Shah (2017). 'Julia: A fresh approach to numerical computing'. In: *SIAM Review* 59.1, pp. 65–98. DOI: `10.1137/141000671`.

Biler, Piotr, Cyril Imbert and Grzegorz Karch (June 2011). 'Barenblatt profiles for a nonlocal porous medium equation'. In: *C. R. Math.* 349.11, pp. 641–645. ISSN: 1631-073X. DOI: `10.1016/j.crma.2011.06.003`.

Carillo, J. A., Y. Huang and S. Martin (2014). 'Explicit flock solutions for Quasi-Morse potentials'. In: *European Journal of Applied Mathematics* 25.5, pp. 553–578. DOI: `10.1017/S0956792514000126`.

Carrillo, José A. and Yanghong Huang (2017). 'Explicit equilibrium solutions for the aggregation equation with power-law potentials'. In: *Kinetic and Related Models* 10.1, pp. 171–192. ISSN: 1937-5093. DOI: `10.3934/krm.2017007`.

Cavagna, Andrea, Alessio Cimarelli, Irene Giardina, Giorgio Parisi, Raffaele Santagati, Fabio Stefanini and Massimiliano Viale (June 2010). 'Scale-free correlations in starling flocks'. In: *Proc. Natl. Acad. Sci. U.S.A.* 107.26, pp. 11865–11870. DOI: `10.1073/pnas.1005766107`.

Cipra, Barry A (2000). 'The best of the 20th century: Editors name top 10 algorithms'. In: *SIAM news* 33.4, pp. 1–2. URL: `https://archive.siam.org/pdf/news/637.pdf` (visited on 14/08/2023).

D'Orsogna, M. R., Y. L. Chuang, A. L. Bertozzi and L. S. Chayes (Mar. 2006). 'Self-Propelled Particles with Soft-Core Interactions: Patterns, Stability, and Collapse'. In: *Phys. Rev. Lett.* 96.10, p. 104302. ISSN: 1079-7114. DOI: `10.1103/PhysRevLett.96.104302`.

D'Orsogna, Maria R. (Dec. 2017). *Why do animals form swarms?* URL: `https://ed.ted.com/lessons/why-do-animals-form-swarms-maria-r-d-orsogna` (visited on 12/08/2023).

Danisch, Simon and Julius Krumbiegel (2021). 'Makie.jl: Flexible high-performance data visualization for Julia'. In: *Journal of Open Source Software* 6.65, p. 3349. DOI: `10.21105/joss.03349`.

Favard, Jean (1935). 'Sur les polynômes de Tchebicheff'. French. In: *Comptes Rendus Hebdomadaires des Séances de l'Académie des Sciences, Paris* 200. zbMath: `0012.06205`, pp. 2052–2053. ISSN: 0001-4036.

Greengard, L. and V. Rokhlin (Dec. 1987). 'A fast algorithm for particle simulations'. In: *J. Comput. Phys.* 73.2, pp. 325–348. ISSN: 0021-9991. DOI: `10.1016/0021-9991(87)90140-9`.

Gutleb, Timon S., José A. Carrillo and Sheehan Olver (Dec. 2022a). 'Computation of Power Law Equilibrium Measures on Balls of Arbitrary Dimension'. In: *Constr. Approx.*, pp. 1–46. ISSN: 1432-0940. DOI: `10.1007/s00365-022-09606-0`.

– (Sept. 2022b). 'Computing equilibrium measures with power law kernels'. In: *Math. Comput.* 91.337, pp. 2247–2281. ISSN: 0025-5718. DOI: `10.1090/mcom/3740`.

Huang, Yanghong (Aug. 2014). 'Explicit Barenblatt profiles for fractional porous medium equations'. In: *Bull. London Math. Soc.* 46.4, pp. 857–869. ISSN: 0024-6093. DOI: `10.1112/blms/bdu045`.

Kwaśnicki, Mateusz (Feb. 2017). 'Ten Equivalent Definitions of the Fractional Laplace Operator'. In: *FCAA* 20.1, pp. 7–51. ISSN: 1314-2224. DOI: `10.1515/fca-2017-0002`.

Liu, Dong C. and Jorge Nocedal (Aug. 1989). 'On the limited memory BFGS method for large scale optimization'. In: *Math. Program.* 45.1, pp. 503–528. ISSN: 1436-4646. DOI: `10.1007/BF01589116`.

Magnus, Wilhelm, Fritz Oberhettinger, R. P. Soni and Eugene P. Wigner (Dec. 1967). 'Formulas and Theorems for the Special Functions of Mathematical Physics'. In: *Phys. Today* 20.12, pp. 81–83. ISSN: 0031-9228. DOI: `10.1063/1.3034082`.

Michel, N. and M. V. Stoitsov (Apr. 2008). 'Fast computation of the Gauss hypergeometric function with all its parameters complex with application to the

Pöschl–Teller–Ginocchio potential wave functions'. In: *Comput. Phys. Commun.* 178.7, pp. 535–551. ISSN: 0010-4655. DOI: 10.1016/j.cpc.2007.11.007.

Milne-Thomson, L. M. (Aug. 1945). *A Treatise on the Theory of Bessel Functions.* Vol. 156. 3955. Nature Publishing Group. DOI: 10.1038/156190a0.

Mogensen, Patrick Kofod et al. (Aug. 2023). 'JuliaNLSolvers/Optim.jl: v1.7.7'. In: *Zenodo.* DOI: 10.5281/zenodo.8254057.

Nelder, J. A. and R. Mead (Jan. 1965). 'A Simplex Method for Function Minimization'. In: *Comput. J.* 7.4, pp. 308–313. ISSN: 0010-4620. DOI: 10.1093/comjnl/7.4.308.

Olver, F.W.J., A.B.O. Daalhuis, D.W. Lozier, B.I. Schneider, R.F. Boisvert, C.W. Clark, B.R. Miller and B. V. Saunders (Dec. 2018). *NIST Digital Library of Mathematical Functions.* https://dlmf.nist.gov. DOI: 10.1023/A:1022915830921. (Visited on 18/08/2023).

Olver, Sheehan and Alex Townsend (Aug. 2013). 'A Fast and Well-Conditioned Spectral Method'. In: *SIAM Review.* DOI: 10.1137/120865458.

Pearson, John W., Sheehan Olver and Mason A. Porter (Mar. 2017). 'Numerical methods for the computation of the confluent and Gauss hypergeometric functions'. In: *Numer. Algorithms* 74.3, pp. 821–866. ISSN: 1572-9265. DOI: 10.1007/s11075-016-0173-0.

Prudnikov, A.P., Y.A. Brychkov, I.U.A. Brychkov and O.I. Marichev (1986). *Integrals and Series: More special functions.* Integrals and Series. Gordon and Breach Science Publishers. ISBN: 9782881246821.

Slevinsky, Richard Mikael (July 2023). 'Fast and stable rational approximation of generalized hypergeometric functions'. In: *arXiv.* Preprint. DOI: 10.48550/arXiv.2307.06221.

Sorensen, D. C. (1982). 'Newton's Method with a Model Trust Region Modification'. In: *SIAM Journal on Numerical Analysis* 19.2, pp. 409–426. DOI: 10.1137/0719026.

Waldert, Peter (Aug. 2023). *Dissertation.* GitHub repository. URL: https://github.com/MrP01/Dissertation (visited on 30/08/2023).

Wu, Lei, Jun Zhang, Jason M. Reese and Yonghao Zhang (Oct. 2015). 'A fast spectral method for the Boltzmann equation for monatomic gas mixtures'. In: *J. Comput. Phys.* 298, pp. 602–621. ISSN: 0021-9991. DOI: 10.1016/j.jcp.2015.06.019.

Yoshida, Masaaki (1997). *Hypergeometric Functions, My Love.* Wiesbaden, Germany: Vieweg+Teubner Verlag. ISBN: 978-3-322-90166-8. DOI: 10.1007/978-3-322-90166-8.

List of Figures and Tables

List of Figures

List of Tables

Appendix A – Various Parameters
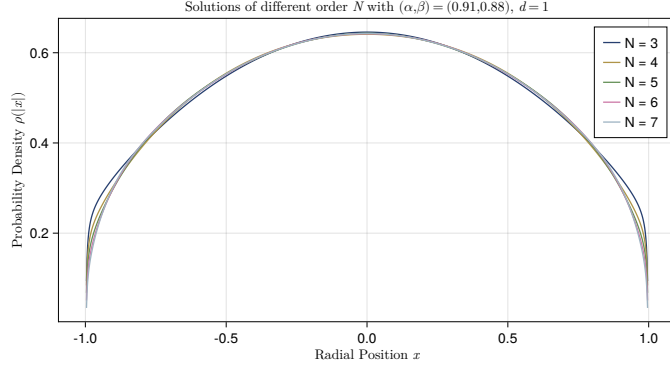
Figure A.1: Solutions with bump parameters.
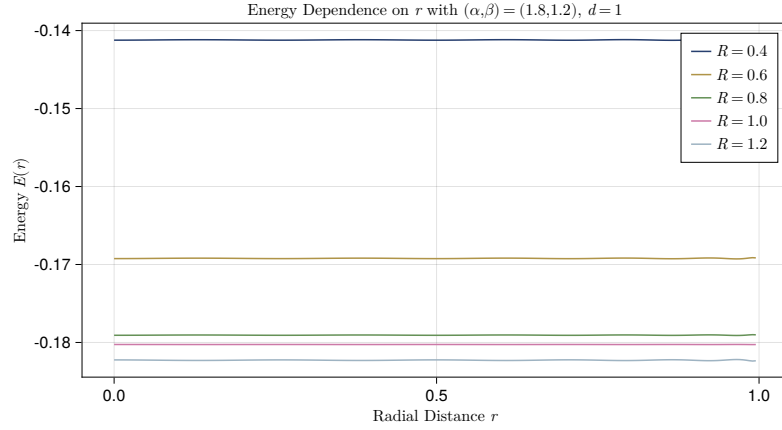
Figure A.2: Plot of the spatial energy dependence on r, for different values of the domain support radius R. As one can see, $\tilde{E}(\boldsymbol{x}) = \boldsymbol{P}^{(a,b)}\left(2\left\|\boldsymbol{x}\right\|_2^2 - 1\right)Q_{\alpha,\beta}\boldsymbol{\rho}$ constant and this figure is only present as visual proof to increase our confidence in the construction of the spectral method.

Appendix B – Code Snippets

```cpp
void ParticleBox::simulate(size_t timesteps) {
  double afterAccelerations[PARTICLES][DIMENSION];
  f(afterAccelerations);
  for (size_t t = 0; t < timesteps; t++) {
    ParticleVectors beforeAccelerations = afterAccelerations;
    memcpy(beforeAccelerations, afterAccelerations, PARTICLES *
    DIMENSION * sizeof(double));
    for (size_t i = 0; i < PARTICLES; i++) {
      for (size_t d = 0; d < DIMENSION; d++)
        positions[i][d] += p.tau * velocities[i][d] + square(p.tau) /
    2 * beforeAccelerations[i][d];
    }

    f(afterAccelerations);
    for (size_t i = 0; i < PARTICLES; i++) {
      for (size_t d = 0; d < DIMENSION; d++) {
        velocities[i][d] += (p.tau / 2 * (beforeAccelerations[i][d] +
    afterAccelerations[i][d])) / p.boxScaling;
      }
    }
    reflectParticles();
  }
}
```